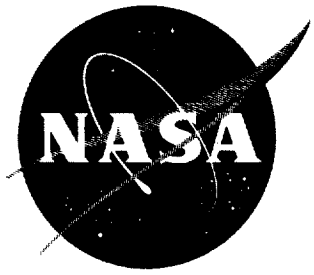

TECHNICAL MEMORANDUM

X-379

EVALUATION OF BLENDED WING-BODY COMBINATIONS WITH CURVED PLAN FORMS AT MACH NUMBERS UP TO 3.50

By George H. Holdaway and Jack A. Mellenthin

Ames Research Center
Moffett Field, Calif.

NATIONAL AERONAUTICS AND SPACE ADMINISTRATION
WASHINGTON

October 1960
Declassified September 1, 1961

NATIONAL AERONAUTICS AND SPACE ADMINISTRATION

TECHNICAL MEMORANDUM X-379

EVALUATION OF BLENDED WING-BODY COMBINATIONS WITH CURVED PLAN FORMS AT MACH NUMBERS UP TO 3.50

By George H. Holdaway and Jack A. Mellenthin

SUMMARY

This investigation is a continuation of the experimental and theoretical evaluation of the effects of wing plan-form variations on the aerodynamic performance characteristics of blended wing-body combinations. The present report compares previously tested straight-edged delta and arrow models which have leading-edge sweeps of 59.04° and 70.82°, respectively, with related models which have plan forms with curved leading and trailing edges designed to result in the same average sweeps in each case. All the models were symmetrical, without camber, and were generally similar having the same span, length, and aspect ratios. The wing sections had an average value of maximum thickness ratio of about 4 percent of the local wing chords in a streamwise direction. The wing sections were computed by varying their shapes along with the body radii (blending process) to match the selected area distribution and the given plan form. The models were tested with transition fixed at Reynolds numbers of roughly 4,000,000 to 9,000,000, based on the mean aerodynamic chord of the wing.

The characteristic effect of the wing curvature of the delta and arrow models was an increase at subsonic and transonic speeds in the lift-curve slopes which was partially reflected in increased maximum lift-drag ratios. Curved edges were not evaluated on a diamond plan form because a preliminary investigation indicated that the curvature considered would increase the supersonic zero-lift wave drag. However, after the test program was completed, a suitable modification for the diamond plan form was discovered. The analysis presented in the appendix indicates that large reductions in the zero-lift wave drag would be obtained at supersonic Mach numbers if the leading- and trailing-edge sweeps are made to differ by indenting the trailing edge and extending the root of the leading edge.

INTRODUCTION

The investigation reported in references 1 and 2 on evaluation of blended wing-body combinations has been extended herein to similar models with curved wing plan forms. The configurations selected were not considered to be optimum, but are useful in demonstrating design variables of possible general application. Thus the wing curvature selected for the delta and arrow models was somewhat arbitrary, but was intended to keep other variables such as aspect ratio, span, volume, and average wing sweeps unaltered. The curvature near the wing tip was roughly of the "Gothic" type described with theoretical calculations in reference 3, which indicated a possibility of reduced strength of the leading-edge vortex for moderately low angles of attack. The wing curvature evaluated was also of interest as a possible means of improving predicted and experimental wave-drag coefficients at supersonic Mach numbers at which a straight-edged plan form would have sonic or supersonic velocities normal to the wing edges.

Experiments were conducted at Mach numbers from 0.60 through 3.50 with transition fixed at Reynolds numbers per foot which varied from about 4,000,000 at transonic speeds to 2,000,000 at Mach numbers of 2.50 through 3.50. The symbols used in the figures are defined in appendix A.

Curved edges are not evaluated for a diamond plan form, because a preliminary investigation indicated that the curvature considered would require abrupt body or wing contouring for sonic design and thus would probably have separated flow drag and increased zero-lift wave drag at supersonic speeds. Another method of modifying the edges, which appears advantageous for a diamond plan form, is discussed in appendix B.

MODELS AND TESTS

Details of the models are presented in figures 1 and 2 and in tables I through V. Although the models with the straight wing edges are completely defined in reference 2, some of the details are repeated here for ready comparison with the models with curved wing edges. The body radii are listed in table I for each model and are different for each model. Note that the delta models do not have the large bump at the rear of the body which was used for some of the tests of reference 2, and thus the delta models have less volume than the arrow models as shown by the area distributions presented in figure 3.

The wing coordinates for the four plan forms are listed in tables II through V. The wing thickness distributions for the curved plan forms are illustrated in figure 2. Similar thickness distributions for the

straight-edged plan forms are presented in reference 2, and for all cases the thicknesses were computed as described in reference 1. The wing thickness is defined by straight-line elements perpendicular to the model center line as shown by the cross sections in figure 2. Note that the arrow wings have blunt trailing edges, as suggested in reference 4, to avoid wing sections with large rearward slopes. For wing sections perpendicular to the body center line, as shown in figure 2(b), the trailing-edge thicknesses of the arrow wings were half the ridge-line thickness, except near the body juncture and the model center line ($y \sim 0$) as shown in tables IV and V. The wing sections had an average value of maximum thickness of about 4 percent of the local chords in a streamwise direction and the thickness ratios were greater inboard.

The curved plan forms were formed by arcs of equal radii for both the leading and trailing edges as shown in figure 1. The arcs near the leading-edge vertex of the delta model were made tangent to the body surface slope at the point of intersection of the straight-edged wing with the body. The arcs at the leading-edge vertex of the arrow model were made to have an included half-angle equal to 10°.

The models were tested at the Ames Research Center in the 14-Foot Transonic Wind Tunnel and in the 9- by 7-foot and 8- by 7-foot supersonic test sections of the Unitary Plan Wind Tunnel. Photographs of the curved models are presented in figure 4, and the arrow model with straight edges is shown in figure 5 in the test section of the 14-Foot Transonic Wind Tunnel. Transition was fixed on all models by means of a distributed roughness. The average size of the grit was 0.040 inch, and the grit was located 1.13 inches rearward of the wing leading edge (upper and lower surfaces) and 1.13 inches rearward of the body nose in a streamwise direction. This location of the grit fixed the amount of laminar flow at 5 percent of the wing area for the entire Mach number range. Selection of the grit was based on the results of references 1 and 2 which indicated that transition would be fixed for the test conditions of this report. The results of reference 2 indicated a drag coefficient penalty due to the grit of about 0.0003 above the increase in the drag coefficients due to fixing transition for the delta model at $M=3.00$. The drag penalty of the grit for the curved plan forms was not measured, but could be slightly greater than the above value because of the increased amount of grit due to the curved line. The arrow model shown in figure 3(b) had transition fixed; however, the grit is difficult to see (located on the white line nearest the wing leading edge).

The ranges of the test variables in each facility are shown in the following table:

Tunnel throat	Models	R/ft	M	α, deg
14-foot	Curved arrow	1,800,000	0.25	-2 to 14
	Delta	3,500,000 to 4,000,000	0.60 to 0.80	-2 to 11
	Curved delta			
	Arrow	4,000,000	0.80 to 1.20	-2 to 8
	Curved arrow			
9- by 7-foot	Delta	4,000,000	1.55	-3 to 5
	Curved delta	3,000,000	1.55 to 2.35	-2 to 12
8- by 7-foot	Delta	3,000,000	3.00	-3 to 13
	Curved delta			
	Arrow	2,000,000	2.50 to 3.50	-3 to 15
	Curved arrow			

Data for the arrow model with straight wing edges were obtained in the 9- by 7-foot test section and are reported in reference 2, but not in the present report because the curved arrow model was not similarly tested in that speed range.

Three-component aerodynamic forces and moments were measured and corrected by standard procedures. For the model sizes and shapes, the force corrections for blockage and buoyancy were generally found to be negligible. At all Mach numbers the drag coefficients were adjusted by equating the body base pressures to free-stream static pressures. All aerodynamic coefficients are based on the complete plan-form area of the wings of 800 square inches. The pitching-moment coefficients were computed about a longitudinal center 34.50 inches rearward from the nose of each model. This position was selected for approximately neutral longitudinal stability at moderately supersonic speeds

RESULTS

The basic test data for the delta and curved delta models are presented jointly in figures 6(a) through 8(d) and for the arrow models in figures 9(a) through 10(d). The Mach numbers listed in the figures are accurate within the decimal places shown, except for the test of the curved arrow model at transonic speeds where the actual test Mach numbers from 0.61 to 1.16 were 0.01 higher than the values listed in figure 9 for the basic arrow model.

Figure 7(e) presents schlieren photographs of the delta model near the wing apex at subsonic and supersonic leading-edge conditions, M=1.55 and 2.35, respectively. Note that at M=2.35 where the leading-edge is theoretically supersonic the shock wave is not attached to the wing leading

edge. Similar schlieren photographs of the curved delta model are shown in figure 7(f). In the case of the curved wing, the wing shock is broken up into a series of smaller shocks, and at M=2.35 the wing shock appears to be detached in the hollow of the wing curve.

The effects of the changes in Reynolds number are illustrated for the curved delta model in figure 7(d) for M=1.55 and in figure 8(d) for M=3.00. The effects of changes in Reynolds number for the curved arrow model are illustrated in figure 10(d). The Reynolds number effects were similarly small for the straight-edged plan forms as shown in reference 2. The wing base-drag coefficients for the two arrow models are presented in figure 9(d) as a function of the lift coefficients. The variation in wing base pressures with spanwise position are presented in reference 2.

DISCUSSION

The discussion is directed primarily toward comparing experimental data of the straight-edged and curved plan forms. The straight-edged delta and arrow models are experimentally and theoretically evaluated along with a diamond model in reference 2. The discussion of the experimental results will consider first the trends with Mach number of maximum lift-drag ratio, lift-curve slope and aerodynamic-center position; and second, the zero-lift wave-drag coefficients of the models. Theoretical wave-drag coefficients were computed for the curved delta model, so that a representative indication of the effect of wing curvature on the theoretical wave drag could be demonstrated with the delta models. All the data presented are with transition fixed and include a grit drag-coefficient penalty of at least 0.0003 (see ref. 2).

Aerodynamic Trends with Mach Number

The basic aerodynamic parameters of the delta and curved delta models are compared in figure 11, and similar data for the arrow models are presented in figure 12. The characteristic effect of the wing curvature was an increase at subsonic and transonic speeds in the lift-curve slopes (ΔC_{L_α} = 0.002 to 0.007 per deg) which was partially reflected in increased maximum lift-drag ratios. At supersonic speeds there was little effect on these parameters as a result of wing curvature.

The wing curvature resulted in a more rearward location of the aerodynamic center position as shown in figures 11(c) and 12(c). In general, the variation in pitching-moment coefficient with lift coefficient was more linear for the wings with curved edges than for the wings with straight edges, as may be noted in the (c) parts of figures 6 through 10.

Zero-Lift Wave-Drag Coefficients

The effect of wing curvature on the zero-lift wave-drag coefficients is small, as may be seen in figure 13. The airfoils were sufficiently sharp that even the straight-edged plan form did not have a rise in zero-lift wave-drag coefficient at supersonic leading-edge conditions. This is more clearly shown by the comparison of experimental and theoretical (computed with the method of ref. 5 using 49 harmonics) wave-drag coefficients of the delta and curved delta models shown in figure 14. Even the theory for the delta model shown in figure 14(a) indicated negligible peaks in the wave drag at sonic leading- and trailing-edge conditions. For wings with blunter leading edges, the agreement between theory and experiment for the straight-edged plan form at supersonic leading-edge conditions would have been poor as was shown in reference 6.

CONCLUDING REMARKS

The characteristic effect of the wing curvature investigated with delta and arrow models was an increase at subsonic and transonic speeds in the lift-curve slopes which was partially reflected in increased maximum lift-drag ratios.

Curved edges were not evaluated on a diamond plan form because a preliminary investigation indicated that the curvature considered would increase the supersonic zero-lift wave drag. However, after the test program was completed, a suitable modification for the diamond plan form was discovered. The analysis presented in the appendix indicates that large reductions in the zero-lift wave drag would be obtained at supersonic Mach numbers if the leading- and trailing-edge sweeps are made to differ by indenting the trailing edge and extending the root of the leading edge.

Ames Research Center
National Aeronautics and Space Administration
Moffett Field, Calif., June 7, 1960

APPENDIX A

NOTATION

A	aspect ratio
b	model span
C_D	drag coefficient (All aerodynamic coefficients are based on the total wing area.)
C_{D_f}	friction drag coefficient
$\frac{C_{D_i}}{C_L^2}$	slope of the curve of drag coefficient due to lift versus lift coefficient squared, taken at the lift-coefficient data point nearest that for $(L/D)_{max}$
C_{D_o}	zero-lift drag coefficient
$C_{D_{wb}}$	wing base drag coefficient
C_L	lift coefficient
C_{L_α}	lift-curve slope, per deg
C_m	pitching-moment coefficient about body station 34.50 inches from the body nose measured in the conventional x direction
c	local wing chord measured in a streamwise direction
c_R	center-line chord
$\bar{c}$	mean aerodynamic chord of the wings with straight leading and trailing edges
$\left(\frac{L}{D}\right)_{max}$	maximum lift-drag ratio
l	model length
M	Mach number
N	total number of harmonics used to compute ΔC_{D_o}

R	Reynolds number
r_b	body base radius
S_w	total wing area
t	wing thickness
V	total model volume
X	airfoil percent-thickness term in NACA 65(06)A00X, airfoil designation
x,y,z	conventional axes measured from the nose of the body or of the wing section
$\frac{x_1}{c_R}$	aerodynamic-center location, where x_1 is measured in the x direction from the leading edge of the wing center-line chord
α	angle of attack
β	$\sqrt{M^2-1}$
ΔC_{D_o}	zero-lift wave-drag coefficient
θ	roll angle of a cutting plane tangent to a Mach cone as measured between the Z axis and the intersection of the cutting plane with the YZ plane

Subscripts or Abbreviations

LE	wing leading edge
TE	wing trailing edge
dia	diamond
max	maximum
mod dia	modified diamond
S.I.L.E.	sonic inboard leading edge
S.I.T.E.	sonic inboard trailing edge

S.O.L.E. sonic outboard leading edge

S.O.T.E. sonic outboard trailing edge

APPENDIX B

ANALYSIS OF A POSSIBLE MODIFICATION TO A DIAMOND PLAN FORM

Reference 1 shows that the symmetry of the diamond plan form was an asset for the blended wing-body type of design at transonic speeds. The data of reference 2 indicated that at higher supersonic speeds the diamond, arrow, and delta plan forms were sufficiently similar in their aerodynamic characteristics that variations in zero-lift wave drag usually decided which model had the highest lift-drag ratio. The possible improvements in supersonic zero-lift wave-drag coefficients are the greatest for the blended diamond wing-body combination because the structural rigidity of the diamond plan form would permit a thinner wing, and the sonic-edge effects could be reduced by sweeping the wing in steps.

The effects of these possible improvements are illustrated in an analysis of two hypothetical models shown in figure 15. The diamond wing plan form is identical with that used for the blended wing-body investigation. The modified diamond plan form of the same aspect ratio was designed as shown in figure 15 with anticipated lift and drag-due-to-lift characteristics similar to the mean of the values for the blended diamond and delta models (which were similar, see ref. 2). A somewhat larger body (von Kármán ogive to body station 60, cylinder to body station 80) was introduced to maintain the model volume, even with thinner wings, equal to or in excess of that used for the blended wing-body investigation. The wing sections considered had the general shapes illustrated in figure 16 which shows one of the thinner thickness-to-chord ratios of 2 percent. The "cycloidal" airfoil is a scaled down cycloid, and was selected because its shape could be expressed analytically and was representative of the wing section at the mean aerodynamic chord of the blended diamond wing. The other wing sections considered were scaled down versions of the NACA 65A006 sections.

Theoretical zero-lift wave-drag coefficients for the hypothetical models with various wing-section shapes and thicknesses are presented in figures 17(a) through 17(c). The theoretical computations are based on the procedures of reference 5, and answers are based on harmonic solutions involving 49 terms. The required area distributions were also machine computed. With the diamond plan form (fig. 17(a)) there was a peak in the theoretical wave-drag coefficient at the combined sonic leading-edge and sonic trailing-edge conditions ($M = 1.414$) even for the thinnest wing section ($(t/c)_{max} = 0.01$). With the thickest "cycloidal" section computed, the peak at sonic edge conditions is beyond the scale of the figure. This thick wing, with maximum section thicknesses of 4 percent of the local chord at the model center line and 8 percent thick at the quarter-span position, was selected as a possible short take off and landing (STOL) configuration

which would have a fan in each wing panel. The results of figure 17(a) indicate that this STOL configuration with a thick wing could possibly be successful at transonic speeds, but probably would not be successful at supersonic leading-edge conditions because of the high wave drag.

The effectiveness of the modification to the diamond plan form in eliminating the peaks in the theoretical zero-lift wave-drag coefficients at sonic edge conditions is demonstrated in figure 17(b) with the same "cycloidal" sections as those used in figure 17(a). It is interesting to note in figure 17(b) that the modified diamond wing, with $(t/c)_{max} = 0.02$ at the model center line and $(t/c)_{max} = 0.01$ at $b/4$ and at the tip, has both greater volume and lower wave drag than a similar model with the thicknesses reversed with the greater thickness ratios at the wing tip. It is of course a well-known fact (see ref. 1) that for low wave drag and low wave drag increase with Mach number, the wing volume should be concentrated inboard.

The "cycloidal" sections with forward and rearward symmetry are good at transonic speeds from a wave-drag standpoint; however, a wing section with less volume near the trailing edge such as the NACA $65_{(06)}$A00X sections would result in lower theoretical wave-drag coefficients at sonic trailing-edge conditions as shown in figure 17(c). For this figure two intermediate wing thicknesses of possible interest were introduced to cover the range of thicknesses more adequately. The 1 percent thick wing was not computed for figure 17(c), because its wave-drag coefficients would be very similar to those shown in figure 17(b) for the 1 percent thick cycloidal wing with the same plan form. Note again in figure 17(c), for two examples (one for thin wings and the other for thick wings) that the wings with the larger thickness ratios inboard not only have the greater volume but also the lower values of wave drag.

The differences between the two airfoil shapes considered were more evident in the initial computation plots of the wave-drag coefficients as a function of $\beta \cos \theta$, as shown in figure 18 for some of the thinner wings. In this type of plot the adverse wave-drag coefficient peaks at sonic edge conditions are more evident. Figure 18 indicates that the "cycloidal" sections are generally poorer with higher wave-drag parameters and are only slightly advantageous for Mach number near 1.00 ($\beta \cos \theta = 0$). This will be shown more clearly in subsequent figures with thicker wings.

The modified diamond plan form resulted in reductions in theoretical zero-lift wave-drag coefficients even for the thinner wing sections as shown in figure 19. The effects of the plan-form modification were of course much greater for the thicker wings as shown in figure 20 with a coarser scale. Note again in this figure that the "cycloidal" sections are better at transonic speeds.

None of the hypothetical models were optimum in any sense, but the models with thin wings and modified plan form were designed to have a continuously decreasing wave-drag coefficient with increasing Mach number similar to that obtained with elliptic wings. Theoretical zero-lift wave-drag coefficients for the hypothetical modified diamond model with several wing thicknesses are compared in figure 21 with similar values from reference 1 or 2 for the blended diamond wing-body combination. It is apparent that the thicker winged, blended wing-body combination designed for Mach number 1.00 is an efficient configuration at transonic speeds; however, the modified diamond configurations are preferred at supersonic edge conditions.

The theoretical zero-lift wave-drag coefficients for a hypothetical modified diamond model, the blended diamond model, and elliptic wings of comparable volumes are compared in figure 22 with experimental results from reference 2 for the blended diamond model. The volume is greatest for the hypothetical modified diamond model, although its wing sections are the thinnest ($(t/c)_{max}$ = 0.02 at center line, $(t/c)_{max}$ = 0.01 at b/4, and $(t/c)_{max}$ = 0.01 at the tip). The possible reductions in zero-lift wave-drag coefficients are very large relative to the blended diamond wing-body combination at supersonic leading-edge conditions. For example at Mach number 2.00 (see fig. 22), the zero-lift wave-drag coefficients might be reduced to less than one-seventh of the experimental results. An increase in maximum lift-drag ratio would naturally result from such modifications; however, the effect would be less impressive than that indicated for the wave drag as shown in the following table.

Experimental results for the blended diamond wing-body combination $\left(\frac{V^{2/3}}{S_w} = 0.112\right)$						
M	Transition	C_{D_i}/C_L^2	C_{D_f}	ΔC_{D_o}	$(L/D)_{max}$	$(R/ft)\times10^{-6}$
2.00[a]	Fixed	0.444	0.00597	0.00645	6.65	3
3.00	Fixed	.730	.00524	.00512	5.80	3 or 4
3.00	Free	.730	.00400	.00512	6.29	4
					6.22	3
Estimated results for the hypothetical modified diamond model $\left(\frac{V^{2/3}}{S_w} = 0.152\right)$						
2.00	Fixed	.433	.00597	.00085	9.21	
3.00	Fixed	.722	.00490	.00065	7.90	
3.00	Free	.722	.00429	.00065	8.36	
3.00[b]	Free	.722	.00429	.00065	7.51	

[a] Read from faired data between M = 1.95 and M = 2.10

[b] Drag increased on the assumption that the increase in base area over that for the experimental model was not filled by engine exhaust, that is, increase in C_{D_o} = 0.00121.

Note that the experimental wave-drag coefficients for the blended diamond model are of the same order of magnitude as the friction-drag coefficients; however, the wave-drag coefficients for the hypothetical model at Mach number 3.00 are of the order of magnitude of almost one-tenth of the friction-drag coefficients. Thus attempts to improve the zero-lift wave-drag coefficients over the theoretical values indicated in the prior table do not seem to be warranted for these models unless the friction-drag coefficients could be similarly reduced.

REFERENCES

1. Holdaway, George H., Mellenthin, Jack A., and Hatfield, Elaine W.: Investigation at Mach Numbers of 0.20 to 3.50 of a Blended Diamond Wing and Body Combination of Sonic Design But With Low Wave-Drag Increase With Increasing Mach Number. NASA TM X-105, 1959.

2. Holdaway, George H., and Mellenthin, Jack A.: Investigation at Mach Numbers of 0.20 to 3.50 of Blended Wing-Body Combinations of Sonic Design With Diamond, Delta and Arrow Plan Forms. NASA TM X-372, 1960.

3. Smith, J. H. B.: A Theory of the Separated Flow From the Curved Leading Edge of a Slender Wing. British, R.A.E. TN Aero 2535, 1957.

4. Chapman, Dean R.: Reduction of Profile Drag at Supersonic Velocities by the Use of Airfoil Sections Having a Blunt Trailing Edge. NACA TN 3503, 1955.

5. Holdaway, George H., and Mersman, William A.: Application of Tchebichef Form of Harmonic Analysis to the Calculation of Zero-Lift Wave Drag of Wing-Body-Tail Combinations. NACA RM A55J28, 1956.

6. Holdaway, George H., Lazzeroni, Frank A., and Hatfield, Elaine W.: Effects of Outboard Thickened and Blunted Leading Edges on the Wave Drag of a 45° Swept-Wing and Body Combination. NASA TM X-27, 1959.

TABLE I.- COORDINATES FOR BODIES, INCHES

Delta model		Curved delta model		Arrow model		Curved arrow model	
x	r	x	r	x	r	x	r
0	0						
.375	.075						
.750	.148						
1.500	.258						
2.250	.356						
3.000	.449						
3.750	.542						
4.500	.623						
5.250	.693						
6.000	.761						
6.750	.830						
7.500	.903						
8.250	.976						
9.000	1.048						
9.750	1.116						
10.500	1.179						
10.683	1.190	10.683	1.190				
11.000	1.210	11.000	1.217				
12.000	1.216	12.000	1.295				
13.000	1.169	13.000	1.374				
14.000	1.099	14.000	1.446				
15.000	1.057	15.000	1.510				
16.000	1.035	16.000	1.560				
16.800	1.026	17.000	1.590				
18.400	1.089	18.000	1.598				
19.200	1.119	19.000	1.578				
20.000	1.149	20.000	1.543				
20.800	1.178	21.000	1.490				
21.600	1.206	22.000	1.447				
23.200	1.260	23.000	1.408				
		24.000	1.372				
24.800	1.311						
		25.000	1.351				
26.400	1.360	26.358	1.357				
28.000	1.405						
29.600	1.447						
31.200	1.487						
32.800	1.522						
33.600	1.539						
34.400	1.554						
35.200	1.569			35.230	1.570	35.675	1.577
36.000	1.582			36.000	1.620	36.000	1.583
36.800	1.594			37.000	1.660	37.000	1.600
37.600	1.605			38.000	1.690	38.000	1.615
38.400	1.614			39.000	1.705	39.000	1.629
39.200	1.621			40.000	1.718	39.746	1.640
40.000	1.625	40.000	1.625	40.500	1.725	40.000	1.642
						40.500	1.650
				41.000	1.735	41.000	1.656
						41.440	1.658
				41.532	1.751	41.532	1.659
				42.000	1.776	42.000	1.675
				43.000	1.821	43.000	1.707
						44.000	1.748
				45.000	1.905	45.000	1.797
						46.000	1.841
				47.000	1.975	47.000	1.881
						48.000	1.920
				49.000	2.011	49.000	1.948
						49.516	1.961
						50.000	1.966
				51.000	2.000	51.000	1.969
						52.000	1.956
				53.000	1.942	53.000	1.933
54.100	1.625					54.000	1.901
54.500	1.637						
55.000	1.651			55.000	1.872	55.000	1.868
56.000	1.681			56.000	1.825	56.000	1.824
57.000	1.711			57.000	1.767	57.000	1.766
				57.500	1.732	57.500	1.733
57.600	1.728			57.600	1.728	57.600	1.728
57.900	1.709						
58.200	1.692						
58.500	1.677						
58.800	1.662						
59.100	1.649						
59.400	1.637						
59.700	1.629						
60.000	1.625						

Equivalent body

Blended body

Cylinder

Fillet

Equivalent body

Wing alone

Blended body

Wing alone

Blended body

(1) Same as Delta Model

(2) von Kármán ogive, l = 40,000 in., r_b = 1.625 in.

TABLE II.- COORDINATES FOR CURVED DELTA WING, INCHES

	Semithickness, ±t/2						
x \ y	0	±2.000	±4.333	±6.667	±10.000	±13.333	±16.667
10.683	0.920						
11.000	.945						
12.000	1.017						
13.000	1.047						
14.000	1.072	14.968=0					
15.000	1.092	.005					
16.000	1.105	.161					
17.000	1.112	.298					
18.000	1.107	.411					
19.000	1.092	.502					
20.000	1.068	.570	20.065=0				
21.000	1.033	.617	.131				
22.000	.992	.645	.241				
23.000	.942	.656	.323	23.081=0			
24.000	.887	.653	.380	.107			
25.000	.820	.632	.413	.193	25.961=0		
26.358	.713	.578	.421	.264	.040		
27.000	.670	.554	.418	.283	.089		
28.000	.623	.526	.412	.299	.137	28.460=0	
29.000	.599	.513	.412	.312	.168	.025	
29.500	.593	.511	.415	.318	.181	.044	
30.000	.586	.507	.415	.323	.192	.060	
30.500	.583	.507	.418	.329	.202	.075	
31.000	.582	.508	.421	.335	.211	.087	
31.500	.585	.512	.427	.342	.221	.100	
32.000	.590	.518	.434	.351	.231	.111	32.358=0
32.500	.596	.525	.442	.359	.240	.122	.003
33.000	.603	.532	.450	.368	.250	.132	.014
33.500	.610	.540	.458	.376	.259	.142	.025
34.000	.618	.548	.466	.384	.268	.151	.034
34.500	.625	.555	.474	.392	.276	.160	.043
35.000	.630	.561	.480	.398	.283	.167	.051
35.500	.634	.565	.484	.404	.289	.174	.059
36.000	.637	.568	.488	.408	.294	.180	.065
36.500	.635	.567	.488	.409	.297	.184	.071
37.000	.632	.565	.487	.410	.298	.187	.076
37.500	.627	.561	.485	.408	.299	.190	.080
38.000	.618	.554	.479	.404	.297	.190	.083
38.500	.607	.544	.471	.398	.294	.190	.086
39.000	.594	.533	.462	.391	.289	.187	.086
39.500	.576	.517	.449	.380	.283	.185	.087
40.000	.558	.501	.435	.370	.275	.181	.087
40.500	.538	.484	.420	.357	.267	.176	.086
41.000	.519	.467	.406	.345	.258	.171	.084
41.500	.488	.439	.382	.325	.243	.162	.080
42.033	.450	.405	.352	.300	.225	.150	.075
42.500	.443	.391	.331	.271	.185	.099	.013
43.000	.408	.355	.293	.232	.144	.055	42.630=0
43.500	.374	.321	.258	.196	.107	.018	
44.000	.340	.288	.226	.165	.078	43.829=0	
44.500	.303	.253	.194	.135	.051		
44.966	.265	.218	.162	.107	.028		
45.500	.230	.185	.133	.081	.006		
46.000	.200	.157	.107	.056	45.648=0		
46.500	.157	.118	.074	.029			
47.000	.121	.085	.044	.002			
47.500	.085	.050	.010	47.033=0			
47.898	.060	.010	47.623=0				
48.700	0	47.933=0					

TABLE III.- COORDINATES FOR DELTA WING, INCHES

	Semithickness, ±t/2						
x \ y	0	±2.000	±4.333	±6.667	±10.000	±13.333	±16.667
8.700	0						
9.000	.540						
9.500	.728						
10.000	.835						
10.600	.920						
11.000	.955						
11.500	.987						
12.000	1.000	12.033=0					
12.500	1.000	.123					
13.000	1.000	.225					
13.500	.992	.303					
14.000	.980	.363					
14.500	.966	.411					
15.000	.948	.447					
15.500	.930	.474	15.922=0				
16.000	.910	.495	.010				
16.500	.888	.508	.066				
17.000	.867	.519	.113				
17.500	.844	.525	.151				
18.000	.822	.526	.184				
18.500	.800	.528	.211				
19.000	.780	.528	.233				
19.500	.765	.529	.254	19.811=0			
20.000	.753	.531	.272	.012			
21.000	.735	.536	.303	.071			
22.000	.723	.542	.330	.119			
23.000	.723	.554	.358	.161			
24.000	.721	.564	.381	.197			
25.000	.719	.572	.400	.229	25.367=0		
26.000	.715	.577	.416	.256	.026		
27.000	.710	.581	.430	.279	.063		
28.000	.706	.584	.442	.300	.096		
29.000	.704	.588	.454	.319	.126		
30.000	.704	.594	.465	.337	.153	30.922=0	
31.000	.707	.601	.478	.355	.179	.002	
32.000	.716	.613	.494	.374	.204	.033	
33.000	.730	.630	.513	.396	.229	.062	
34.000	.739	.642	.528	.414	.252	.090	
35.000	.742	.648	.538	.429	.272	.115	
36.000	.739	.649	.544	.438	.288	.138	
37.000	.721	.636	.537	.438	.296	.155	.013
37.500	.706	.625	.529	.434	.297	.162	.025
38.000	.688	.610	.518	.427	.297	.166	.036
39.000	.643	.573	.490	.407	.289	.172	.054
40.000	.593	.530	.456	.383	.277	.172	.067
41.000	.535	.480	.415	.351	.259	.167	.075
41.500	.506	.455	.395	.335	.249	.163	.077
42.033	.474	.427	.371	.316	.237	.158	.079
42.500	.439	.392	.337	.282	.203	.124	.046
43.000	.400	.353	.299	.244	.166	.088	.010
43.500	.365	.318	.264	.209	.131	.053	43.144=0
44.000	.332	.284	.230	.175	.097	.018	
44.500	.295	.248	.194	.139	.061	44.256=0	
45.000	.261	.214	.159	.104	.026		
45.500	.225	.178	.123	.069	45.367=0		
46.000	.191	.144	.089	.034			
46.500	.155	.108	.053	46.478=0			
47.000	.120	.073	.018				
47.500	.083	.037	47.256=0				
48.000	.050	.002					
48.500	.008	48.033=0					
48.700	0						

TABLE IV.- COORDINATES FOR CURVED ARROW WING, INCHES

Semithickness, ±t/2											
y / x	0	±2.000	±4.333	±6.667	±10.000	±13.333	±16.567	Ridge		Trailing edge	
								±t/2	±y	±t/2	±y
0.000	0.000										
.500	.166										
1.000	.330										
1.500	.397										
2.000	.453										
2.500	.504										
3.000	.544										
3.500	.588										
4.000	.620										
4.500	.655										
5.000	.680										
5.500	.705										
5.750	.716										
6.000	.723										
6.500	.748										
7.000	.767										
7.500	.787										
8.000	.806										
8.855		0.000									
9.000	.843	.017									
10.000	.873	.122									
11.000	.891	.211									
12.000	.900	.285									
13.000	.917	.352									
14.000	.926	.409									
15.000	.948	.465									
16.000	.961	.512									
16.143			0.000								
17.000	.955	.544	.065								
17.500	.952	.559	.100								
18.000	.946	.570	.132								
18.500	.942	.582	.161								
19.000	.936	.591	.189								
19.500	.930	.600	.214								
20.000	.925	.608	.238								
21.000	.918	.625	.282								
21.940				0.000							
22.000	.914	.641	.322	.004							
23.000	.916	.660	.360	.061							
24.000	.921	.679	.396	.114							
25.000	.918	.691	.426	.161							
26.000	.913	.700	.452	.203							
27.000	.903	.704	.472	.240							
28.000	.894	.708	.490	.273							
28.750	.888	.710	.503	.296	0.000						
29.000	.886	.711	.507	.303	.012						
30.000	.881	.716	.523	.330	.055						
31.000	.884	.726	.541	.357	.093						
32.000	.893	.740	.562	.383	.128						
33.000	.909	.759	.585	.411	.161						
33.122	.911	.762	.588	.414	.165			0.911	0.000		
34.000	.887	.778	.607	.436	.192			.887	.509		
34.500	.870	.784	.616	.447	.206			.870	.812		
35.000	.852	.790	.624	.458	.220			.852	1.130		
35.560						0.000					
35.675	.826	.797	.634	.470	.237	.004		.826	1.577		
36.000	.789	.795	.634	.473	.243	.013		.809	1.797		
36.293		[1].793									
36.500	.713	.780	.637	.479	.253	.028		.785	2.146		
37.000	.652	.740	.641	.485	.263	.041		.762	2.505		
37.500	.592	.693	.642	.490	.272	.054		.737	2.874		
38.000	.550	.648	.641	.492	.279	.066		.710	3.257		
38.500	.502	.601	.639	.493	.285	.077		.682	3.645		
39.000	.450	.551	.636	.494	.291	.088		.654	4.039		
39.360			[1].635								
39.500	.392	.498	.621	.495	.296	.097		.627	4.445		

TABLE IV.- COORDINATES FOR CURVED ARROW WING, INCHES - Concluded

Semithickness, ±t/2											
y / x	0	±2.000	±4.333	±6.667	±10.000	±13.333	±16.667	Ridge		Trailing edge	
								±t/2	±y	±t/2	±y
39.746	0.366	0.472	0.595	0.494	0.298	0.102		0.612	4.654	0.366	0.000
40.000		.447	.571	.494	.300	.106		.599	4.863	.353	.244
40.500		.398	.520	.491	.303	.114		.570	5.288	.332	.728
41.000		.335	.462	.486	.304	.121		.538	5.724	.293	1.219
41.440		.276	.410	.482	.304	.126		.512	6.103	.256	1.658
41.532		.269	.403	.483	.306	.128		.509	6.185	.255	1.750
41.779		.251									
42.000			.366	.491	.314	.136		.494	6.610	.247	2.224
42.063				[1].492							
42.500			.327	.456	.322	.146		.478	7.067	.239	2.738
43.000			.289	.415	.332	.156		.462	7.530	.231	3.260
43.500			.252	.375	.341	.164		.446	8.012	.223	3.790
44.000			.215	.336	.350	.173		.430	8.500	.215	4.328
44.004			.215								
44.239							0.000				
44.500				.297	.360	.182	.005	.414	8.994	.207	4.874
45.000				.260	.371	.192	.013	.398	9.493	.199	5.429
45.489					[1].383						
45.500				.224	.382	.203	.022	.383	10.015	.192	5.993
46.000				.188	.343	.213	.031	.367	10.527	.184	6.566
46.087				.182							
46.500					.304	.224	.040	.351	11.048	.176	7.148
47.000					.267	.235	.048	.335	11.555	.168	7.740
47.500					.231	.247	.057	.319	12.058	.160	8.342
48.000					.196	.258	.066	.303	12.550	.152	8.954
48.500					.162	.269	.075	.287	13.032	.144	9.576
48.817						[1].277					
48.838					.138						
49.000						.264	.084	.271	13.505	.136	10.209
49.516						.228	.094	.255	13.985	.128	10.875
50.000						.195	.103	.239	14.417	.120	11.501
50.500						.161	.112	.223	14.864	.112	12.135
51.000						.127	.122	.207	15.295	.104	12.758
51.470						.096					
51.500							.131	.191	15.719	.098	13.370
52.000							.141	.175	16.138	.088	13.973
52.500							.151	.159	16.538	.080	14.565
52.660							[1].154				
53.000							.132	.143	16.938	.072	15.148
53.500							.102	.128	17.325	.064	15.722
54.000							.071	.112	17.693	.056	16.286
54.342							.050				
54.500								.096	18.059	.048	16.842
55.000								.080	18.413	.040	17.389
55.500								.064	18.753	.032	17.927
56.000								.048	19.086	.024	18.457
56.500								.032	19.402	.016	18.979
57.000								.016	19.707	.008	19.494
57.500								.000	20.000	.000	20.000

[1]Ridge

TABLE V.- COORDINATES FOR ARROW WING, INCHES

x \ y	Semithickness, ±t/2										
	0	±2.000	±4.333	±6.667	±10.000	±13.333	±16.667	Ridge		Trailing edge	
								±t/2	±y	±t/2	±y
0.000	0.000										
.500	.086										
1.000	.171										
1.500	.207										
2.000	.237										
2.500	.270										
3.000	.304										
3.500	.337										
4.000	.360										
4.500	.380										
5.000	.395										
5.500	.402										
5.750		0.000									
6.000	.408	.017									
6.500	.414	.048									
7.000	.426	.076									
7.500	.443	.103									
8.000	.467	.131									
9.000	.505	.182									
10.000	.534	.227									
11.000	.552	.263									
12.000	.567	.295									
12.457			0.000								
13.000	.587	.327	.025								
14.000	.610	.359	.067								
15.000	.640	.395	.108								
16.000	.669	.429	.148								
17.000	.688	.455	.184								
17.500	.696	.467	.201								
18.000	.704	.479	.217								
18.500	.712	.491	.233								
19.000	.718	.501	.247								
19.167				0.000							
19.500	.725	.511	.262	.012							
20.000	.731	.521	.276	.030							
21.000	.746	.542	.303	.065							
22.000	.764	.564	.331	.098							
23.000	.789	.592	.362	.131							
24.000	.814	.619	.391	.164							
25.000	.833	.641	.418	.194							
26.000	.851	.663	.443	.224							
27.000	.864	.680	.465	.251							
28.000	.877	.697	.487	.277							
28.750					0.000						
29.000	.890	.714	.508	.302	.008						
30.000	.906	.732	.530	.327	.038						
31.000	.925	.753	.553	.353	.067						
32.000	.948	.778	.579	.380	.096						
33.000	.977	.807	.608	.410	.126						
33.333	.986	.816	.617	.419	.136			0.986	0.000		
34.000	.955	.832	.635	.437	.155			.955	.552		
34.500	.932	.845	.648	.450	.169			.932	.966		

TABLE V.- COORDINATES FOR ARROW WING, INCHES - Concluded

x \ y	Semithickness, ±t/2										
	0	±2.000	±4.333	±6.667	±10.000	±13.333	±16.667	Ridge		Trailing edge	
								±t/2	±y	±t/2	±y
35.000	0.908	0.853	0.657	0.462	0.182			0.905	1.379		
35.230	.898	.855	.661	.466	.188			.891	1.570		
35.750		[1].853									
36.000	.852	.839	.665	.476	.205			.838	2.207		
36.500	.815	.805	.666	.480	.215			.802	2.621		
37.000	.768	.769	.668	.486	.225			.770	3.034		
37.500	.710	.725	.668	.489	.233			.736	3.448		
38.000	.642	.674	.668	.492	.242			.703	3.862		
38.333						0.000					
38.500	.576	.620	.667	.495	.250	.004		.671	4.276		
38.569			[1].667								
39.000	.508	.565	.632	.499	.258	.017		.642	4.690		
39.500	.445	.509	.584	.499	.264	.029		.609	5.103		
40.000	.387	.458	.540	.502	.271	.040		.582	5.517	0.387	0
40.500		.397	.493	.508	.280	.052		.558	5.931	.339	.571
41.000		.338	.441	.508	.285	.062		.530	6.345	.300	1.143
41.389				[1].513							
41.532		.268	.386	.504	.295	.074		.509	6.785	.255	1.750
41.750		.251									
42.000			.350	.468	.306	.085		.494	7.172	.247	2.286
42.500			.314	.432	.318	.096		.478	7.586	.239	2.857
43.000			.277	.395	.329	.108		.462	8.000	.231	3.429
43.791			.218								
44.000				.371	.352	.131		.430	8.828	.215	4.571
45.000				.247	.375	.154		.398	9.655	.199	5.714
45.417					[1].385						
45.833				.186							
46.000					.342	.177		.367	10.483	.183	6.857
47.000					.268	.200		.335	11.310	.167	8.000
47.918							0.000				
48.000					.194	.223	.002	.303	12.138	.151	9.143
48.750					.139						
49.000						.247	.025	.271	12.966	.136	10.286
49.444						[1].257					
50.000						.216	.048	.239	13.793	.120	11.429
51.000						.143	.071	.207	14.621	.104	12.571
51.667						.093					
52.000							.094	.175	15.448	.088	13.714
53.000							.117	.143	16.276	.072	14.857
53.473							[1].128				
54.000							.090	.112	17.103	.056	16.000
54.584							.046				
55.000								.080	17.931	.040	17.143
55.500								.064	18.345	.032	17.714
56.000								.048	18.759	.024	18.286
56.500								.032	19.172	.016	18.857
57.000								.016	19.586	.008	19.429
57.500								.000	20.000	.000	20.000

[1]Ridge

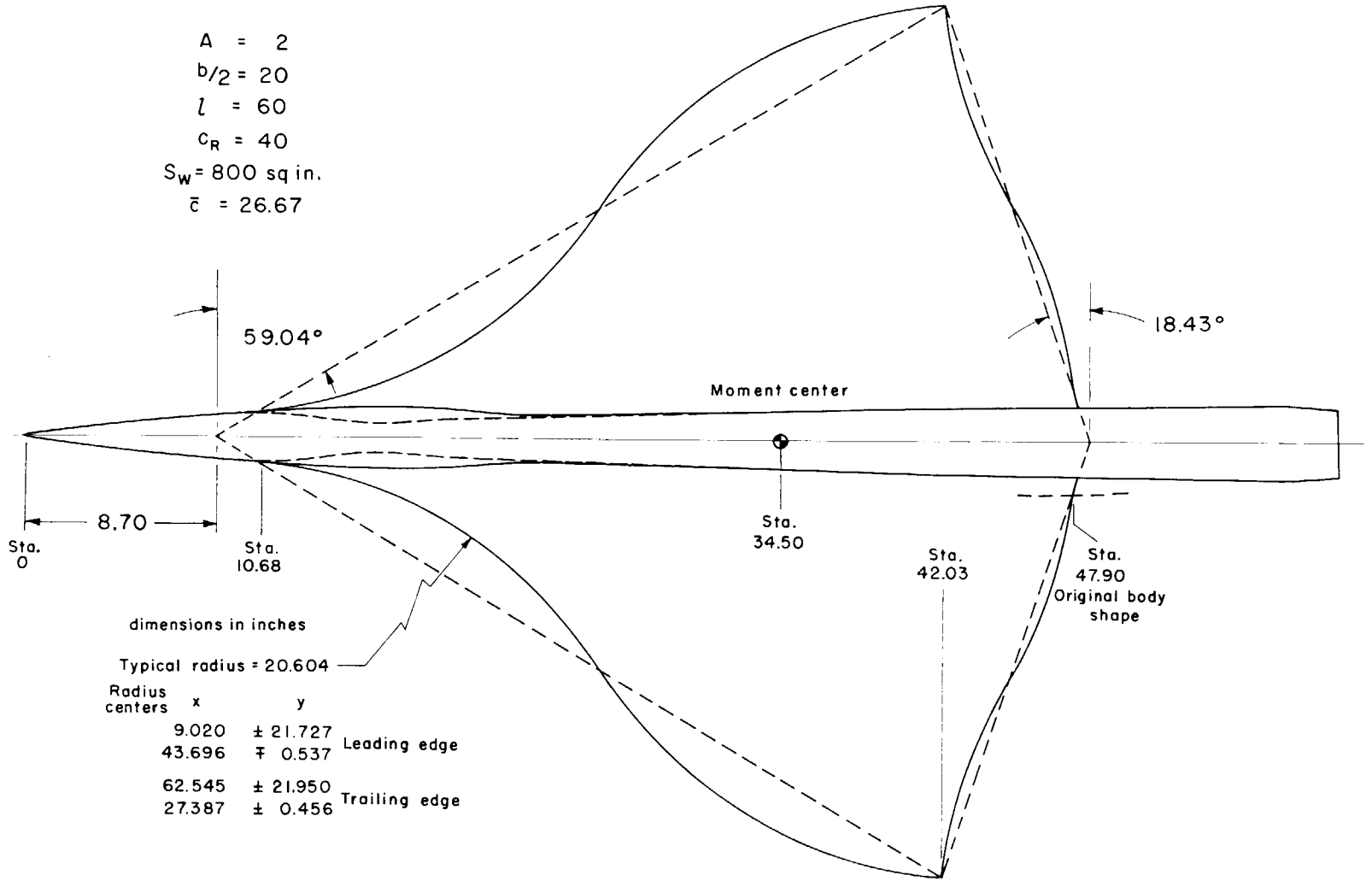

(a) The curved delta model with outline of delta model shown for comparison.

Figure 1.- Sketches of the models.

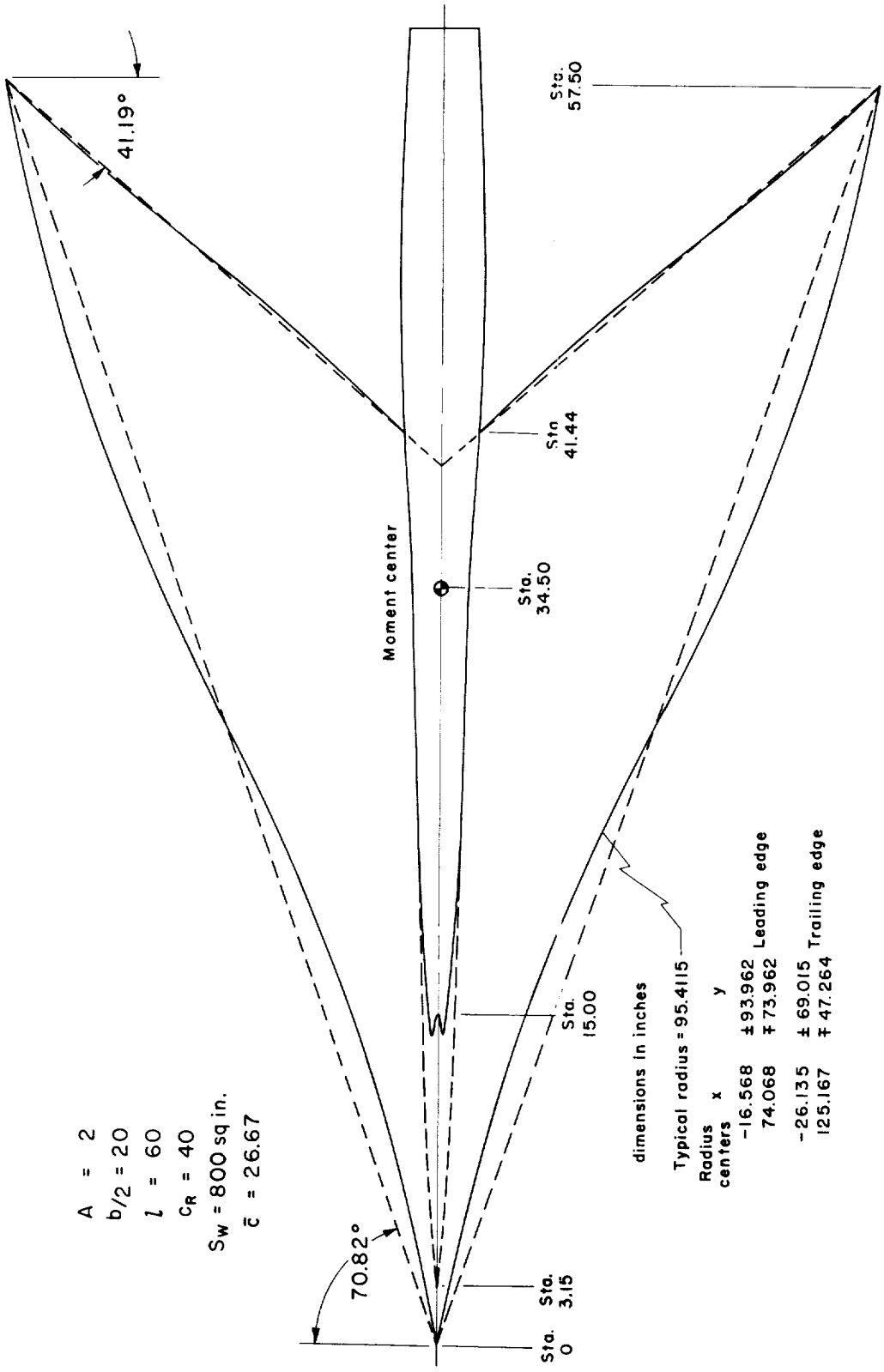

(b) The curved arrow model with the outline of the arrow model shown for comparison.

Figure 1.- Concluded.

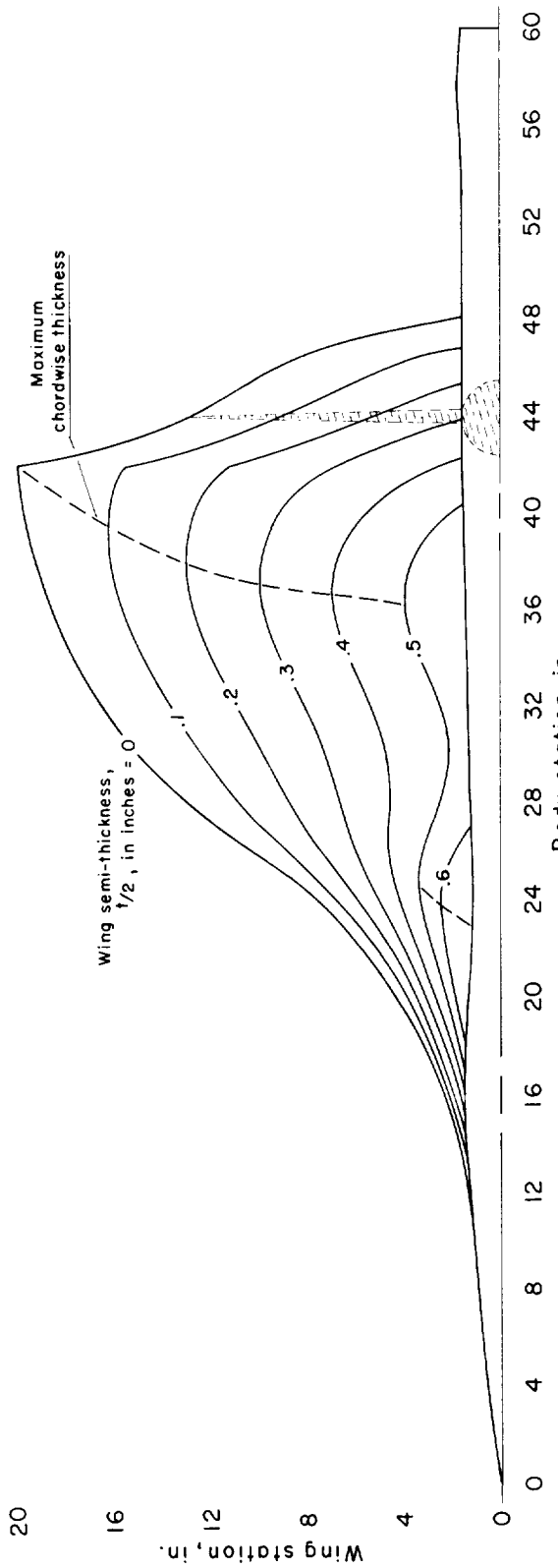

(a) Curved delta model.

Figure 2.- Semi-plan view of the curved models with wing thickness contours.

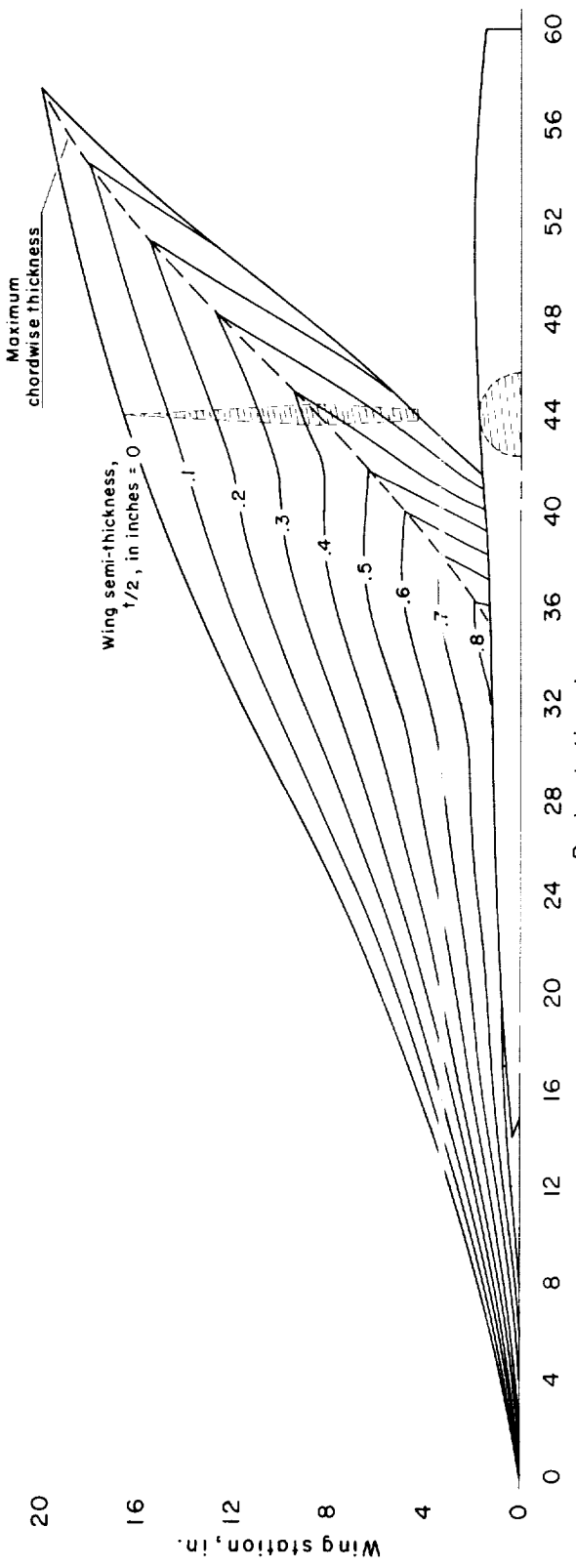

(b) Curved arrow model.

Figure 2.- Concluded.

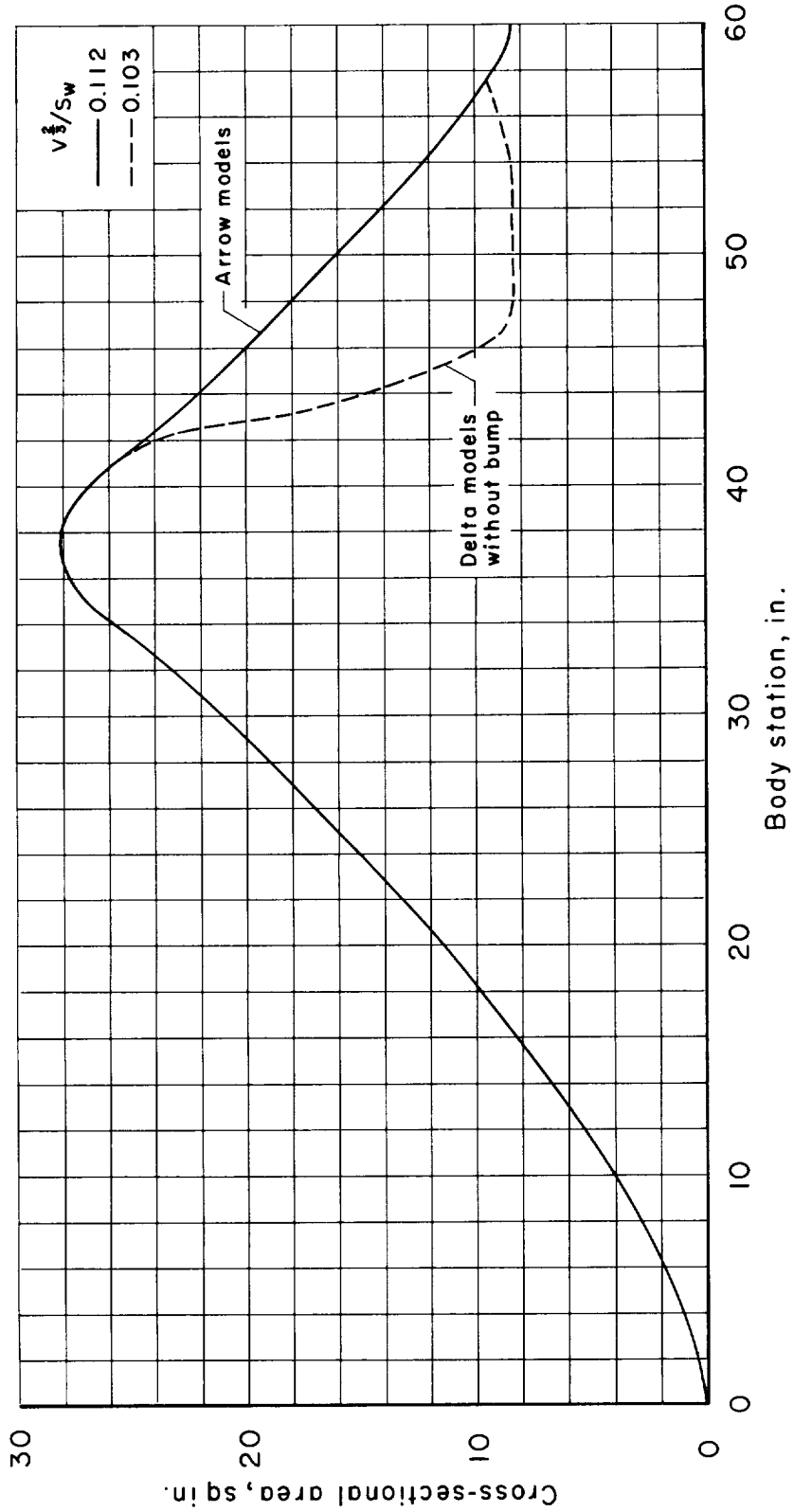

Figure 3.- The design area distribution as derived in reference 1 and modified for the delta models without the body bump.

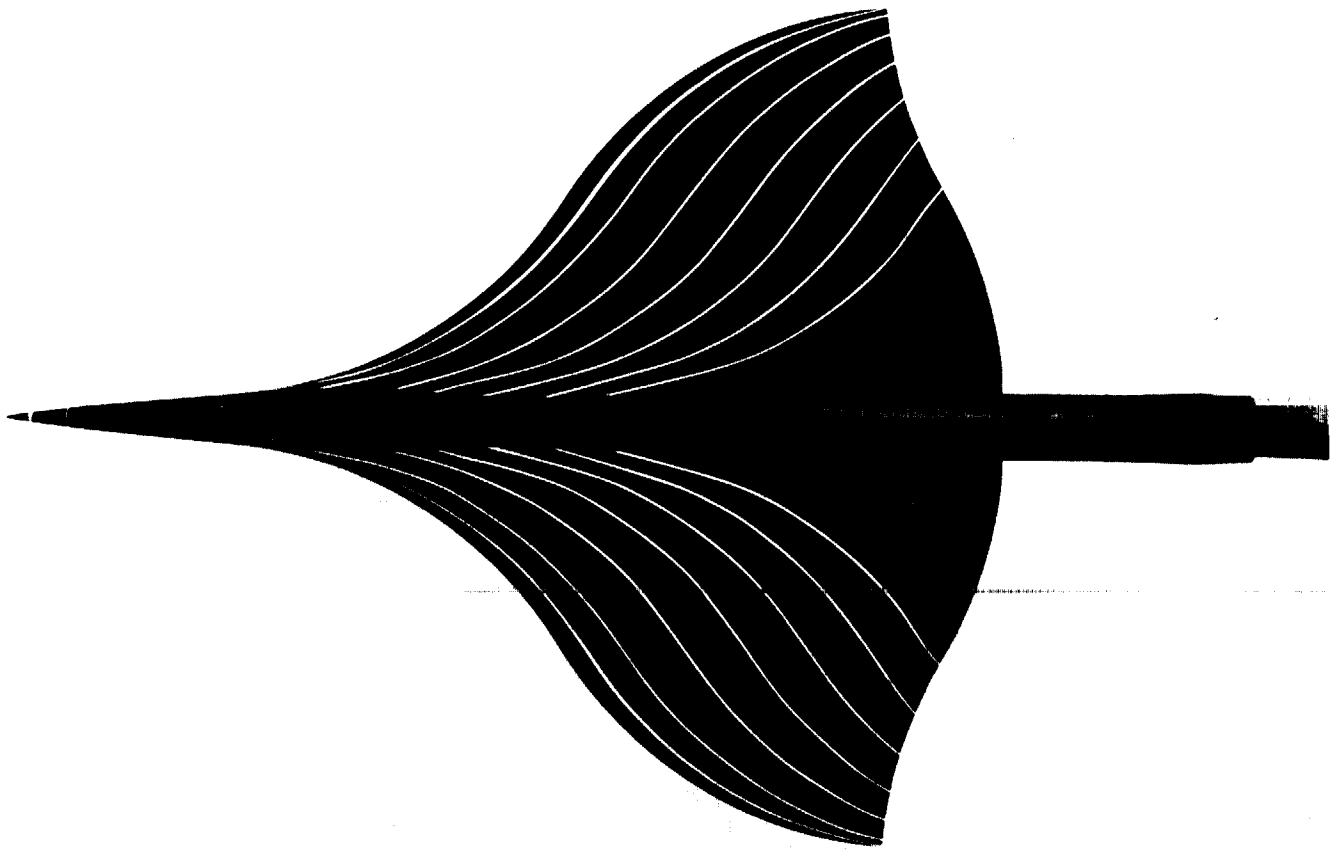

A-24216

(a) Curved delta model.

Figure 4.- Photographs of the curved models.

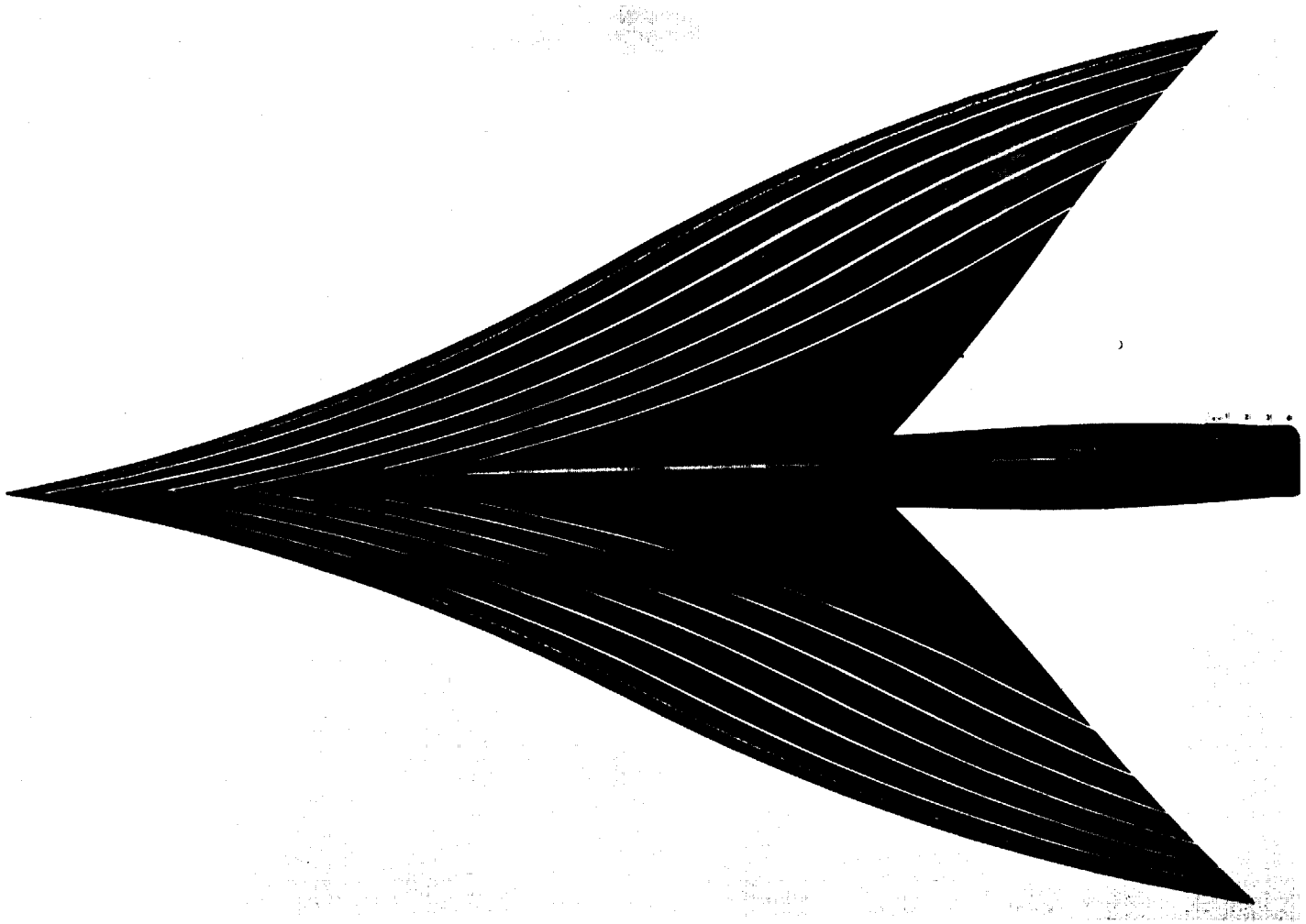

A-24343

(b) Curved arrow model.

Figure 4.- Concluded.

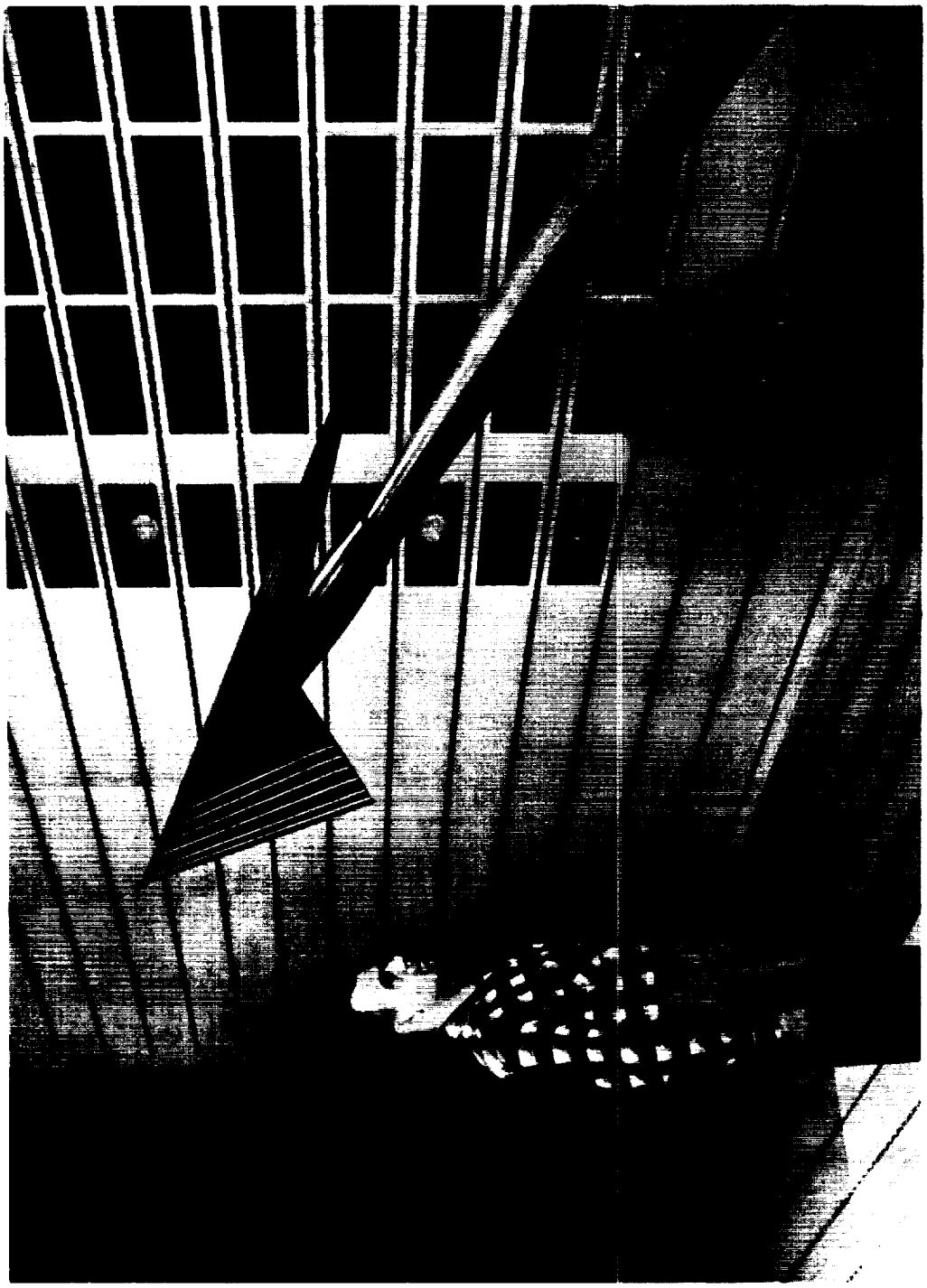

A-23949

Figure 5.- Photograph of the arrow model mounted in the test section of the Ames 14-Foot Transonic Wind Tunnel.

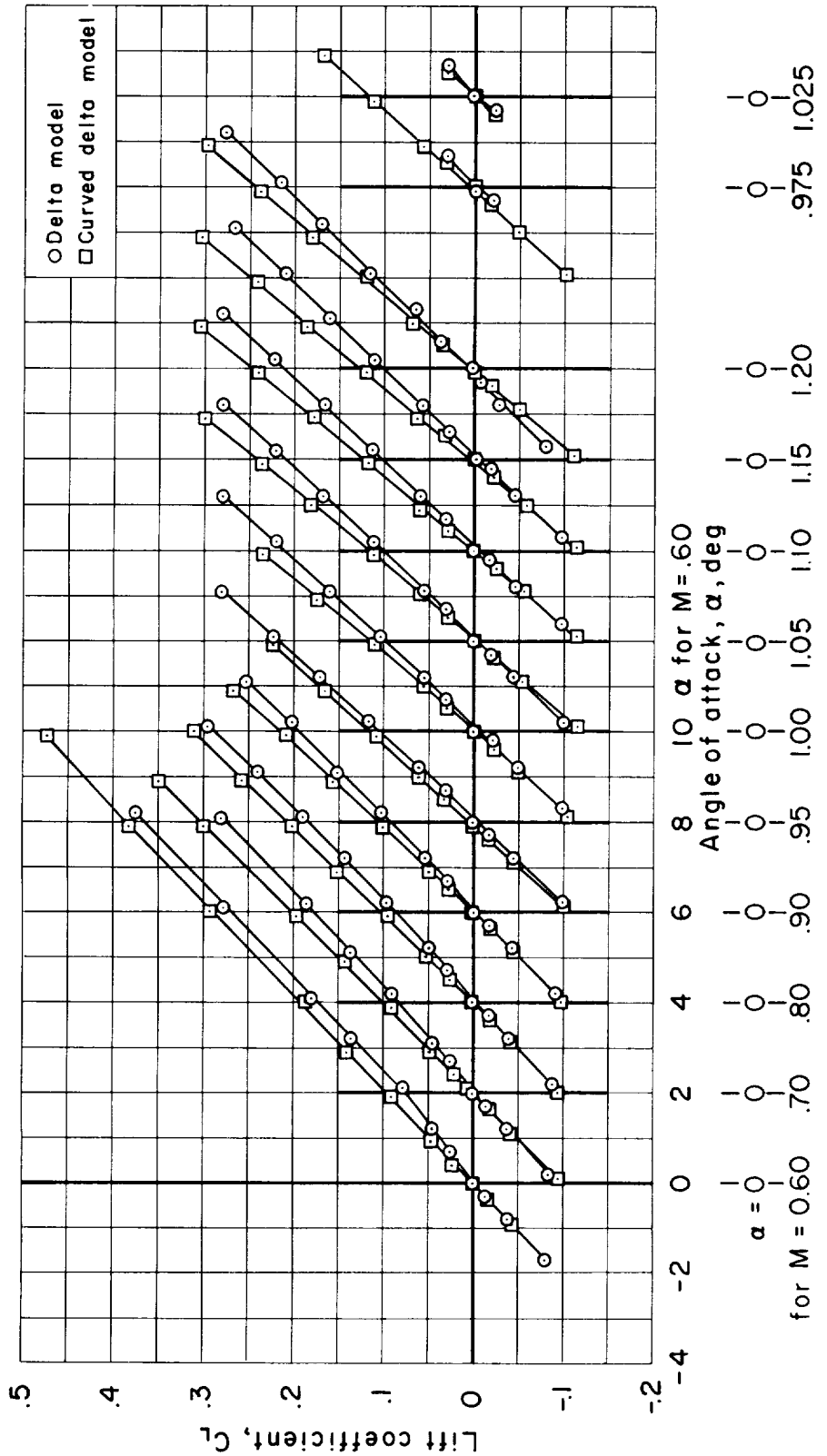

(a) C_L vs. α

Figure 6.- Transonic aerodynamic characteristics for the delta and curved delta models (R/ft = 3,500,000 to 4,000,000).

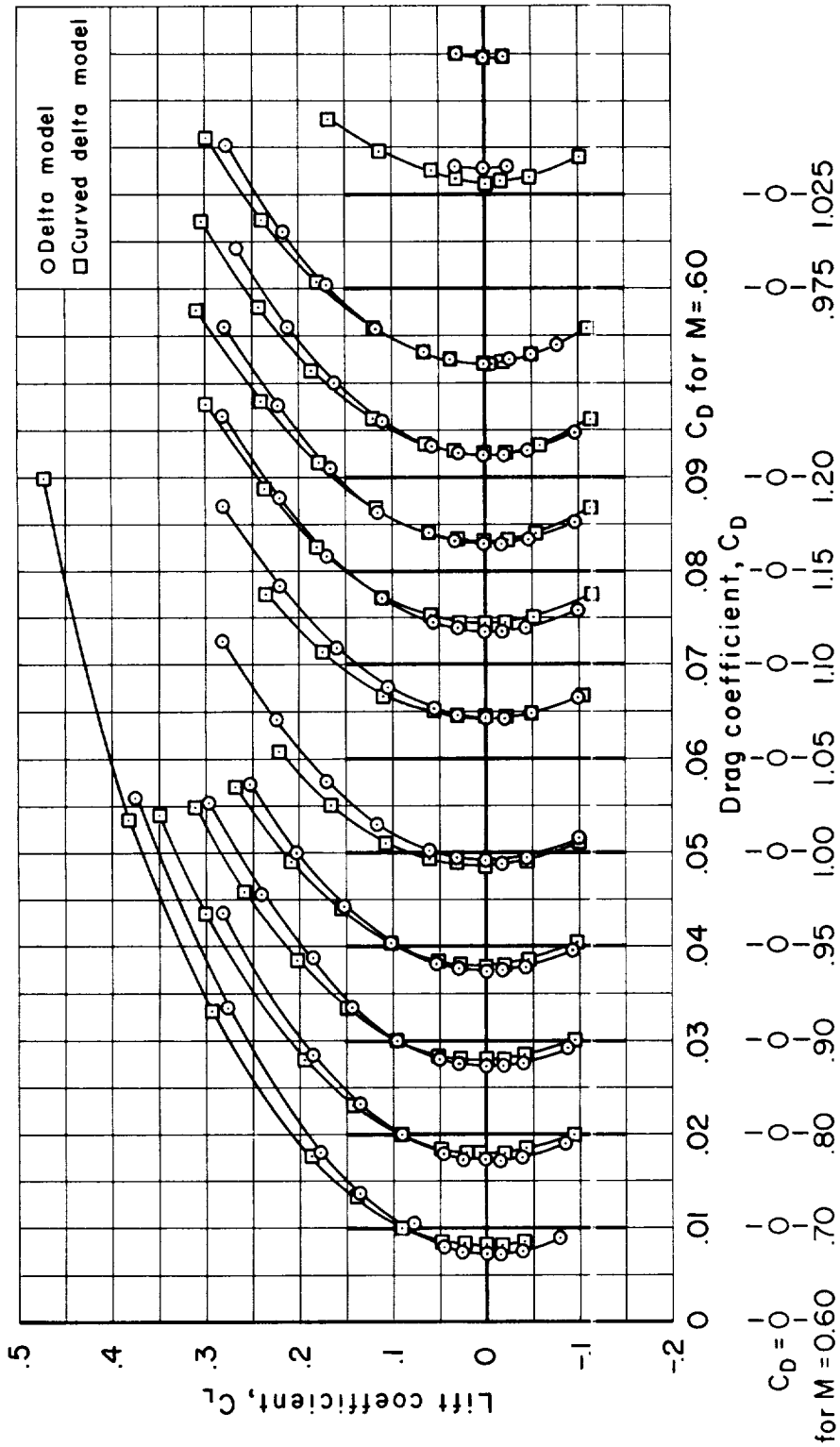

(b) C_L vs. C_D

Figure 6.- Continued.

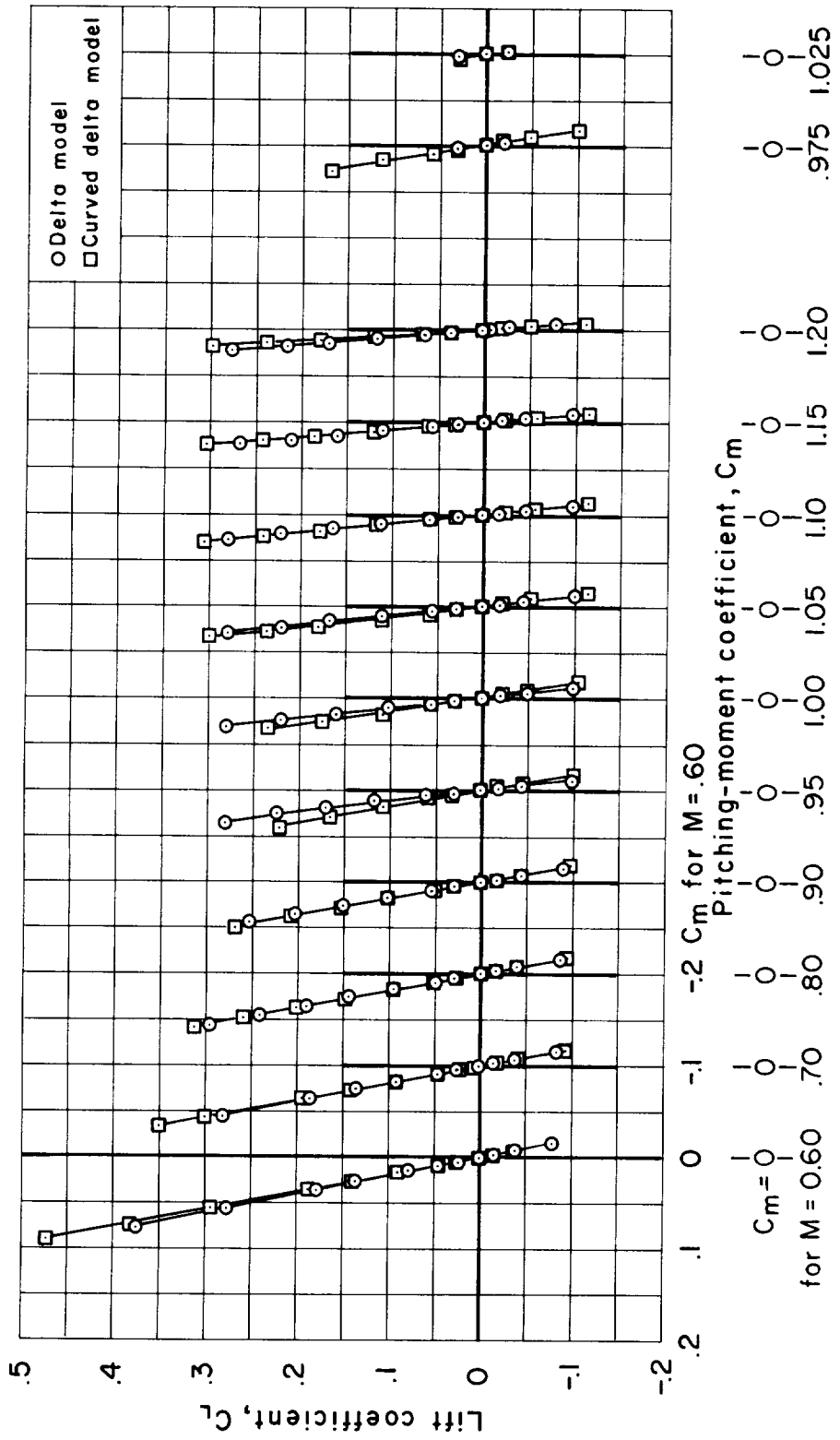

(c) C_L vs. C_m

Figure 6.- Concluded.

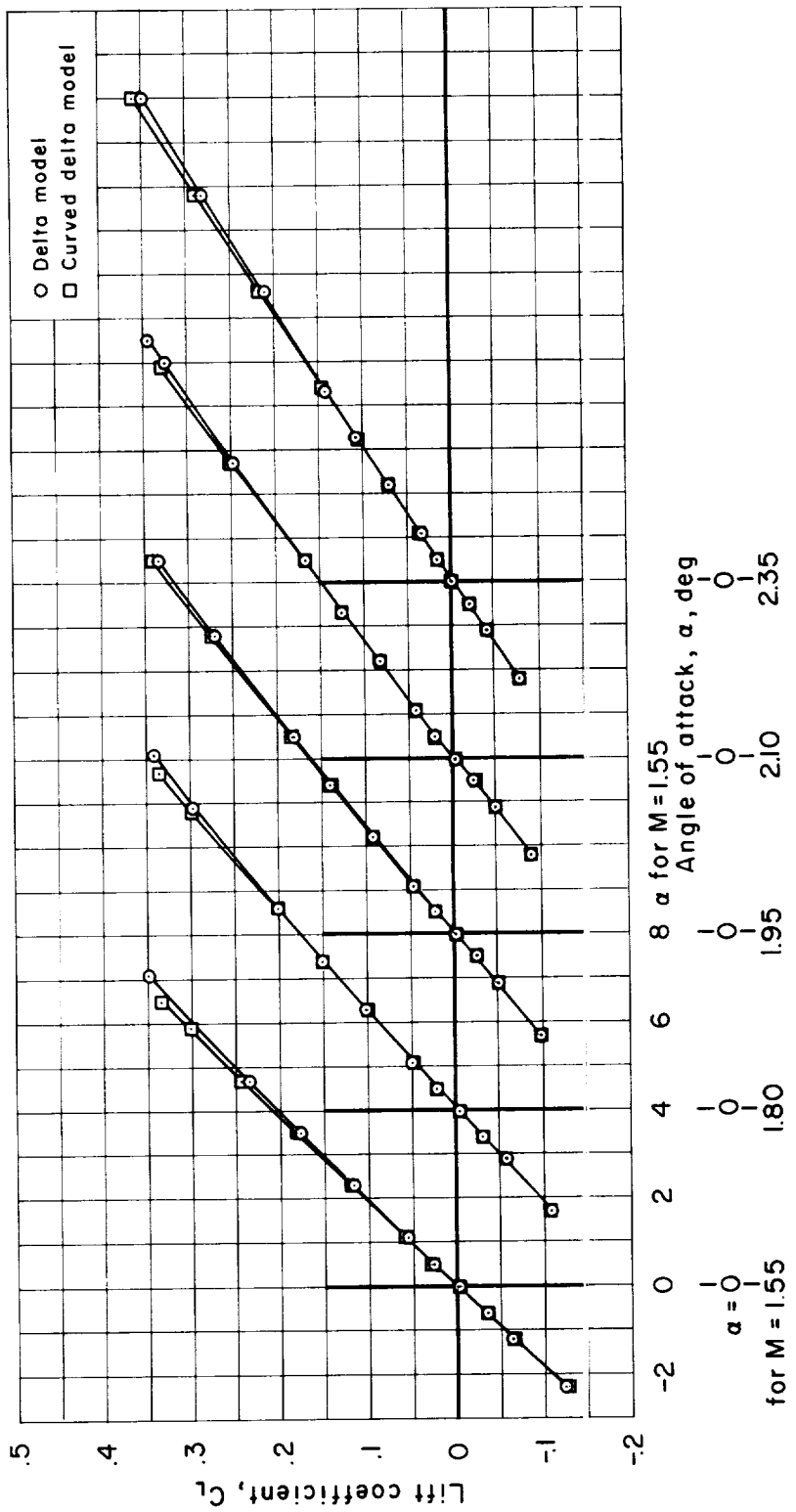

(a) C_L vs. α

Figure 7.- Supersonic aerodynamic characteristics for the delta and curved delta models (R/ft = 3,000,000).

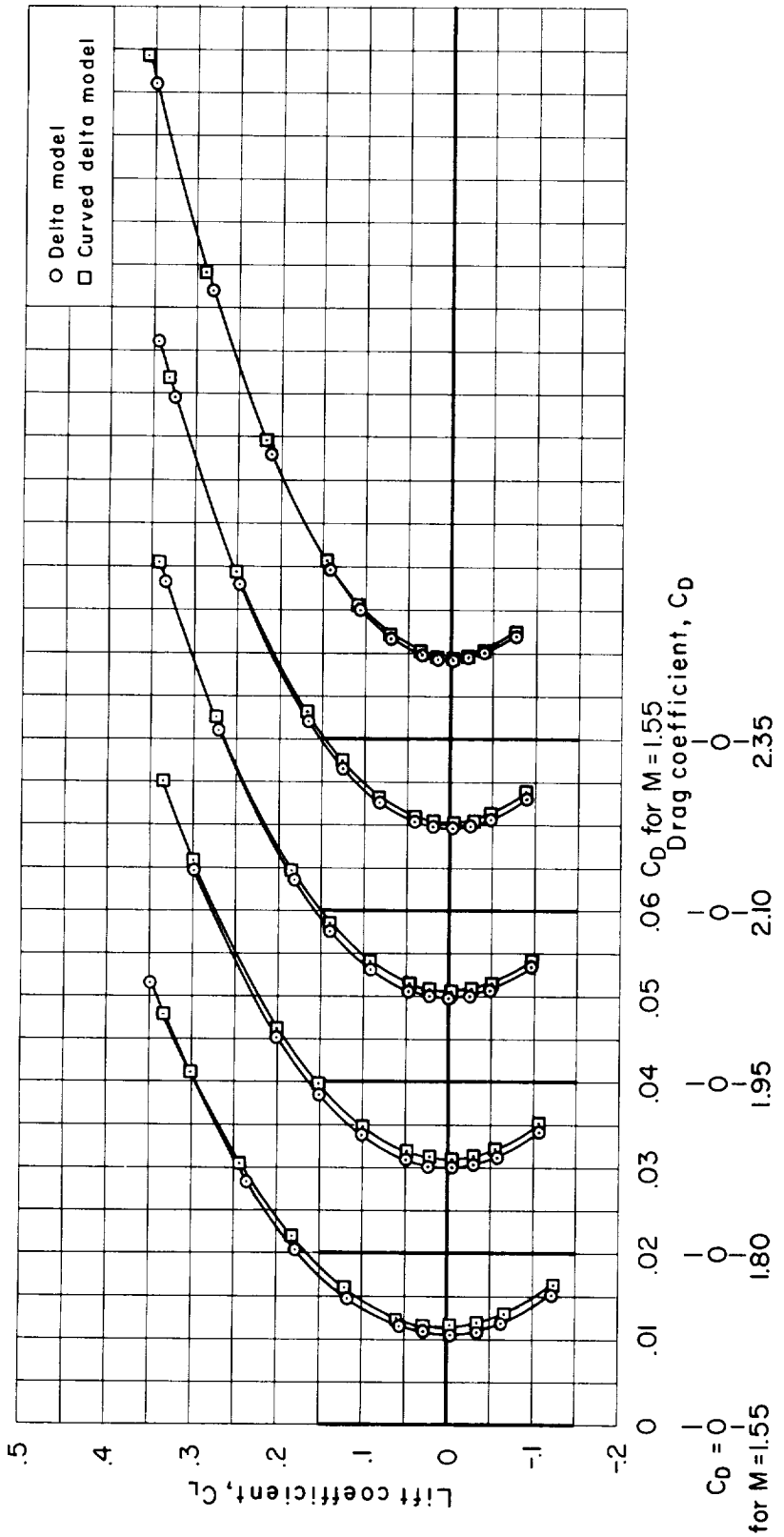

(b) C_L vs. C_D

Figure 7.- Continued.

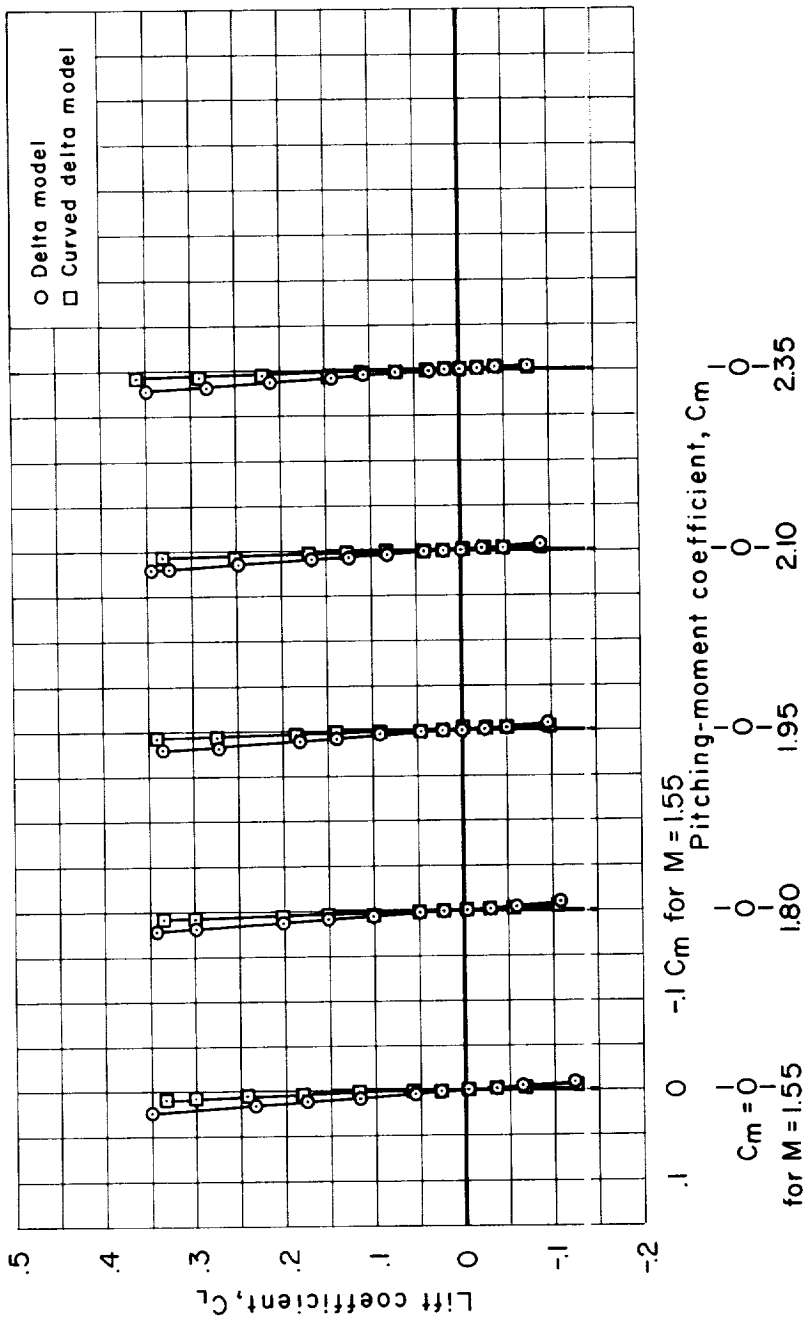

(c) C_L vs. C_m

Figure 7.- Continued.

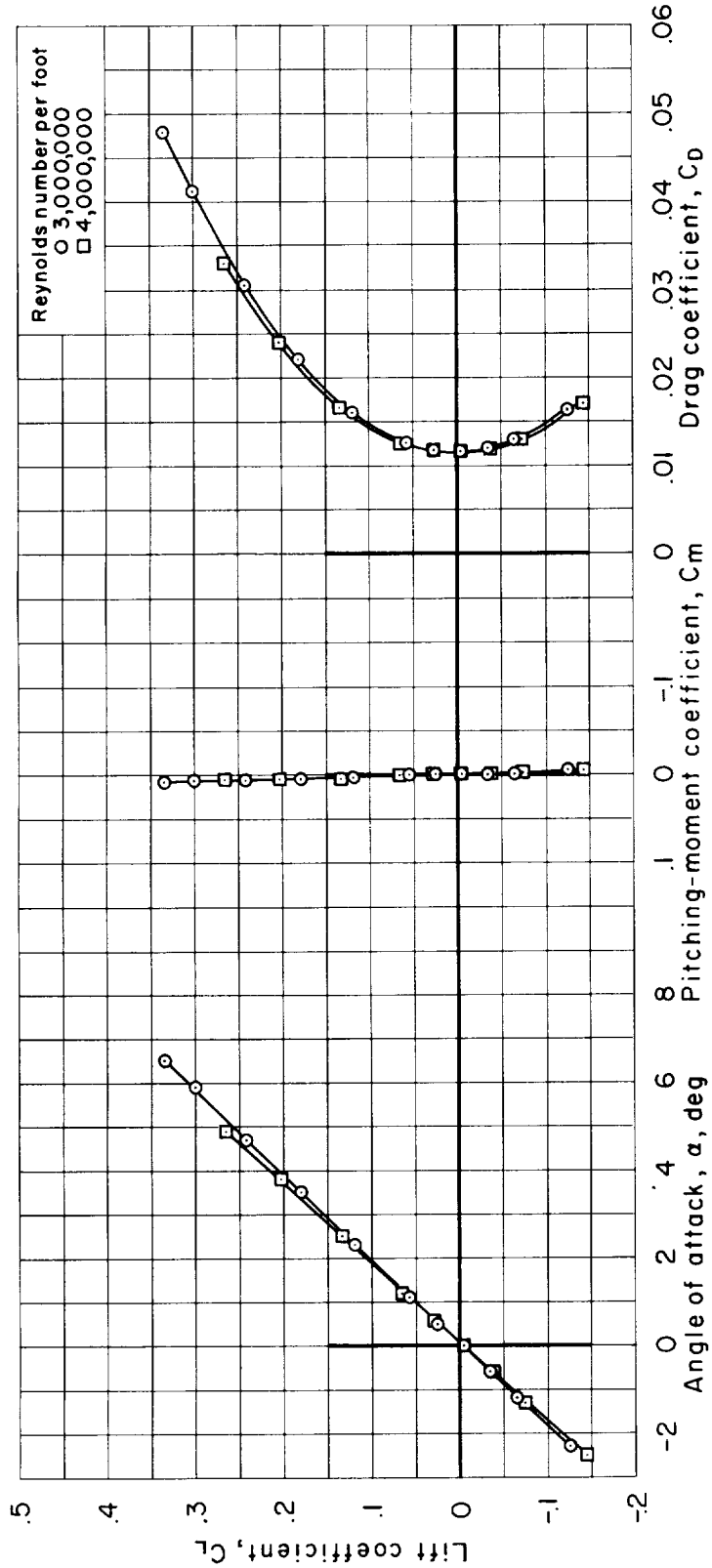

(d) Reynolds number effect at M = 1.55; curved delta model.

Figure 7.- Continued.

Subsonic leading edge

M=1.55

Supersonic leading edge

M=2.35

(e) Schlieren photographs of delta model.

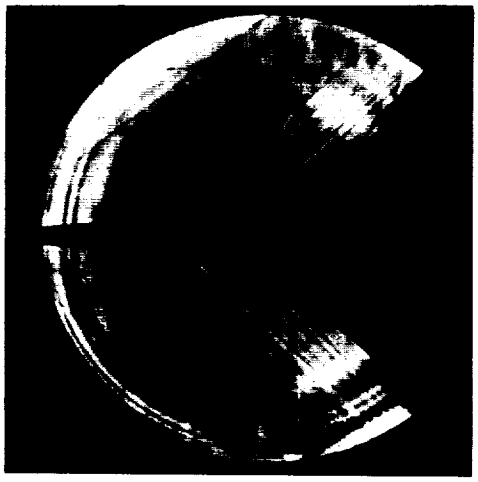

M=1.55

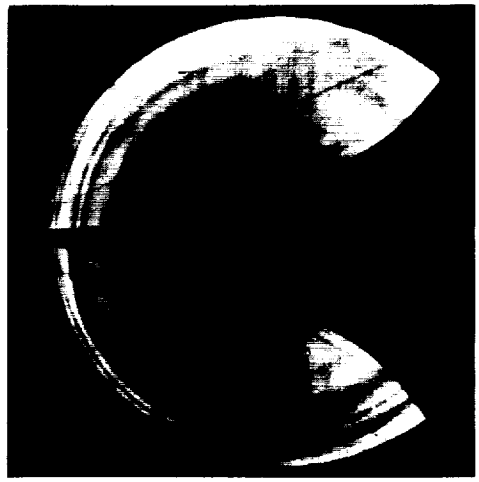

M=2.35

(f) Schlieren photographs of curved delta model.

Figure 7.- Concluded.

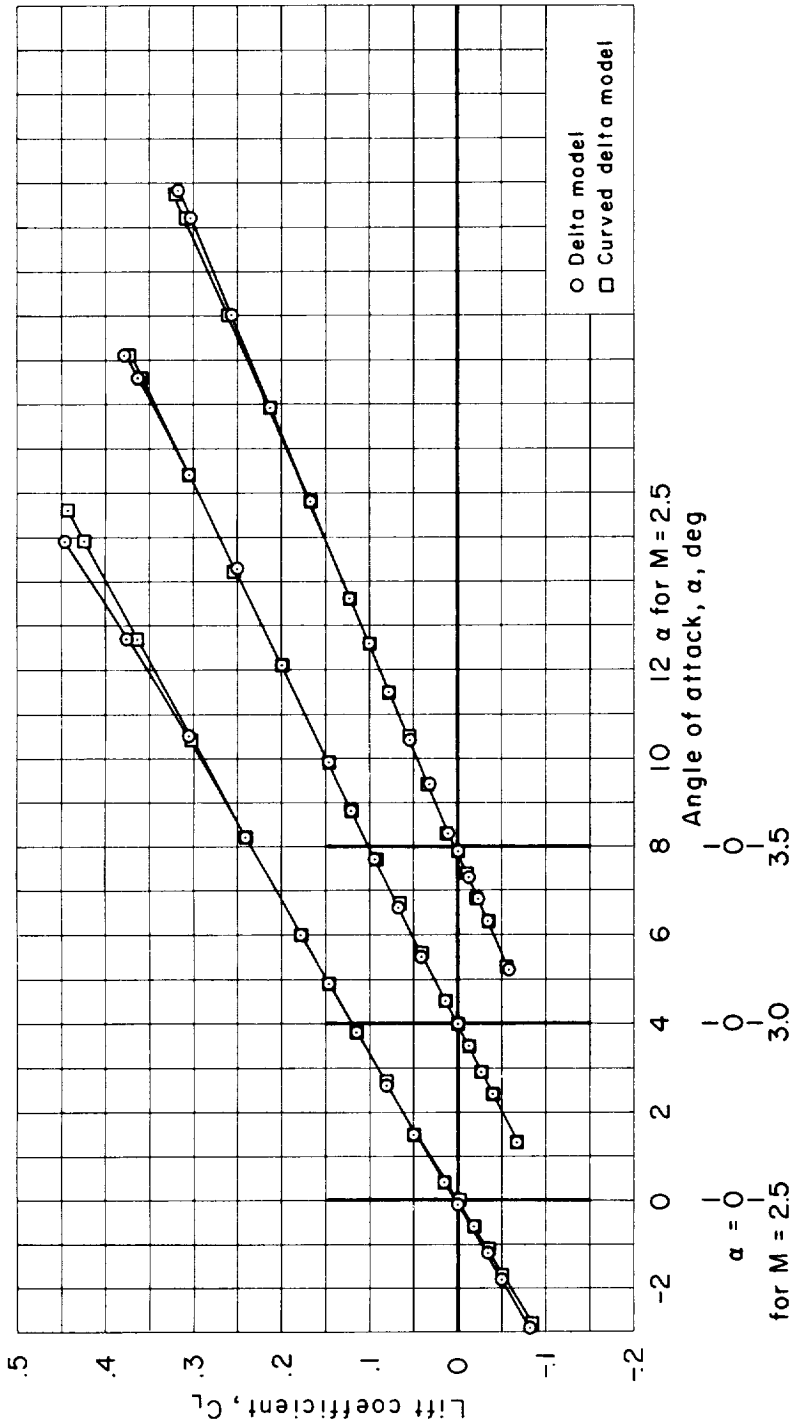

(a) C_L vs. α

Figure 8.- Supersonic aerodynamic characteristics for the delta and curved delta models (R/ft = 2,000,000).

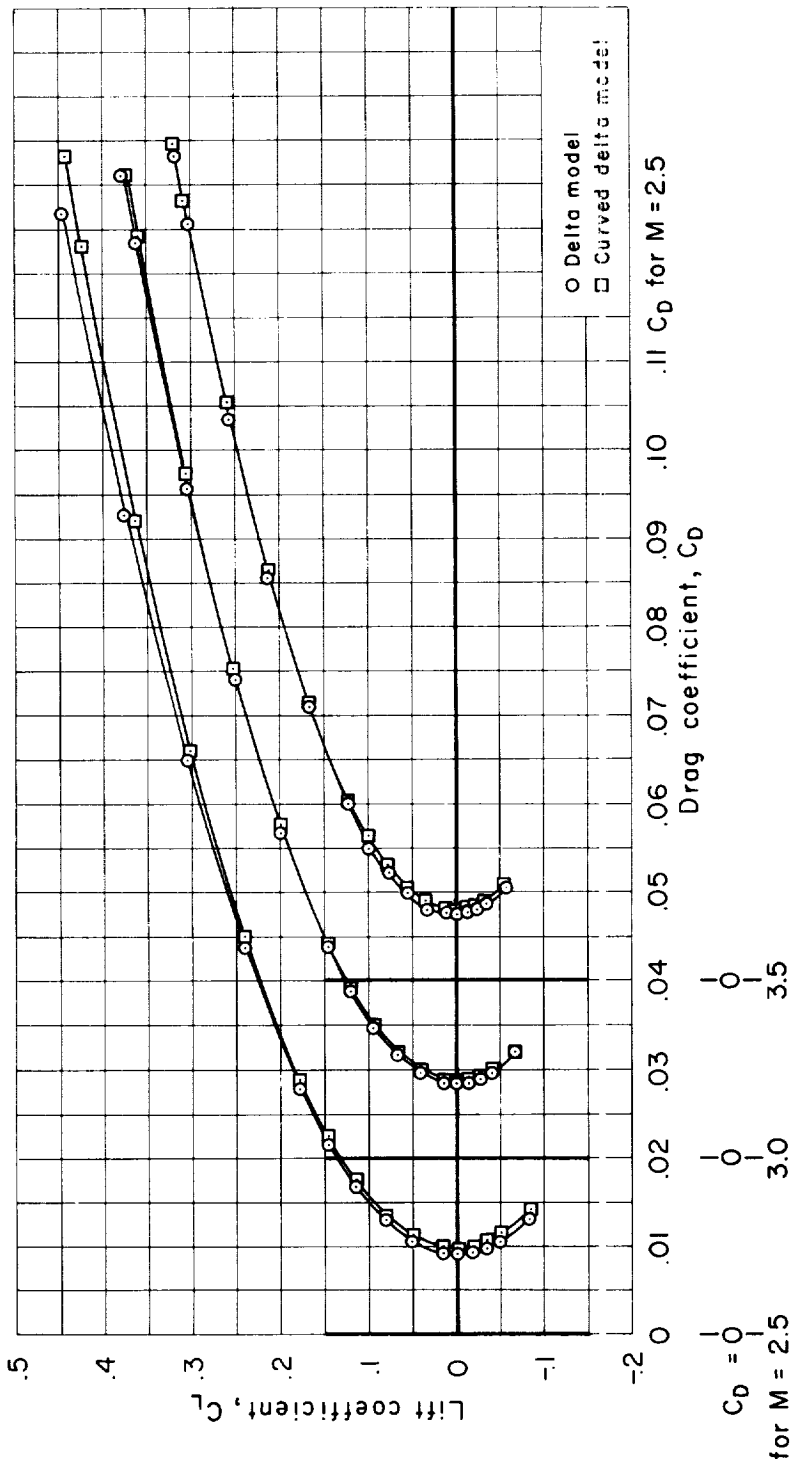

(b) C_L vs. C_D

Figure 8.- Continued.

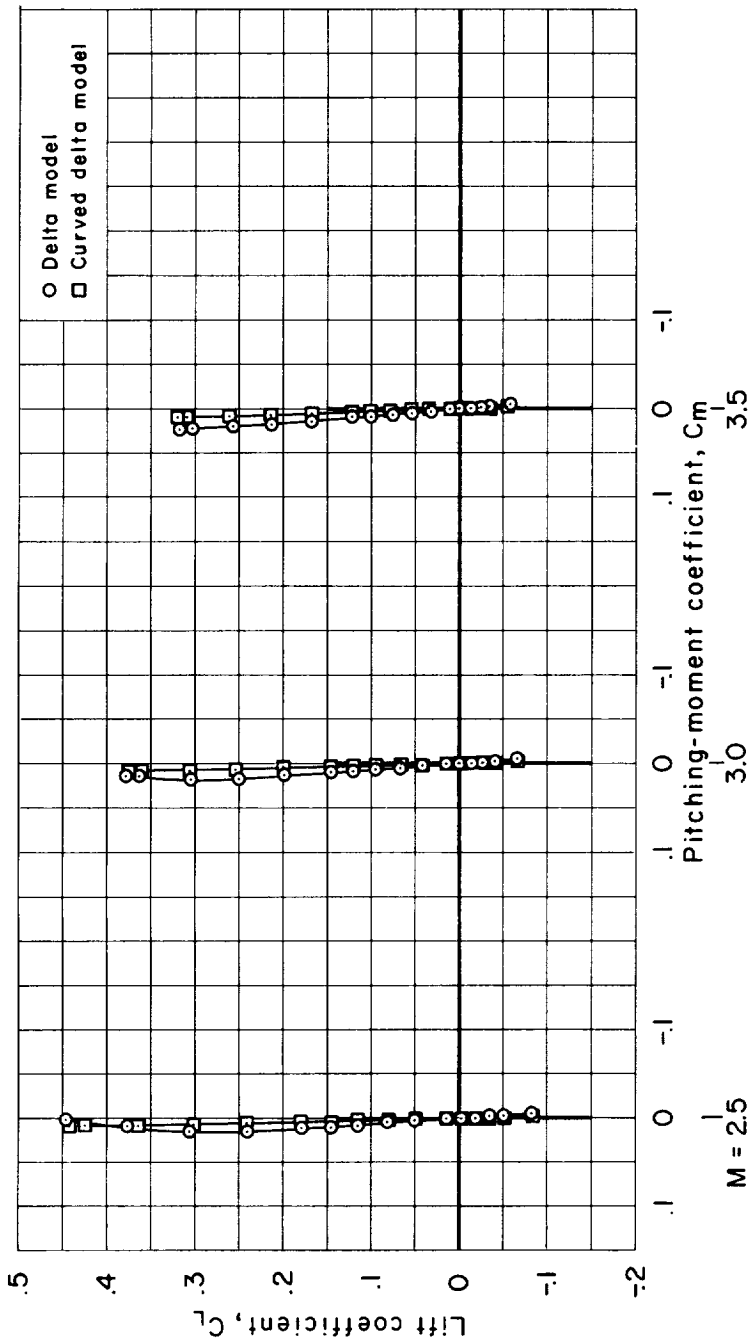

(c) C_L vs. C_m

Figure 8.- Continued.

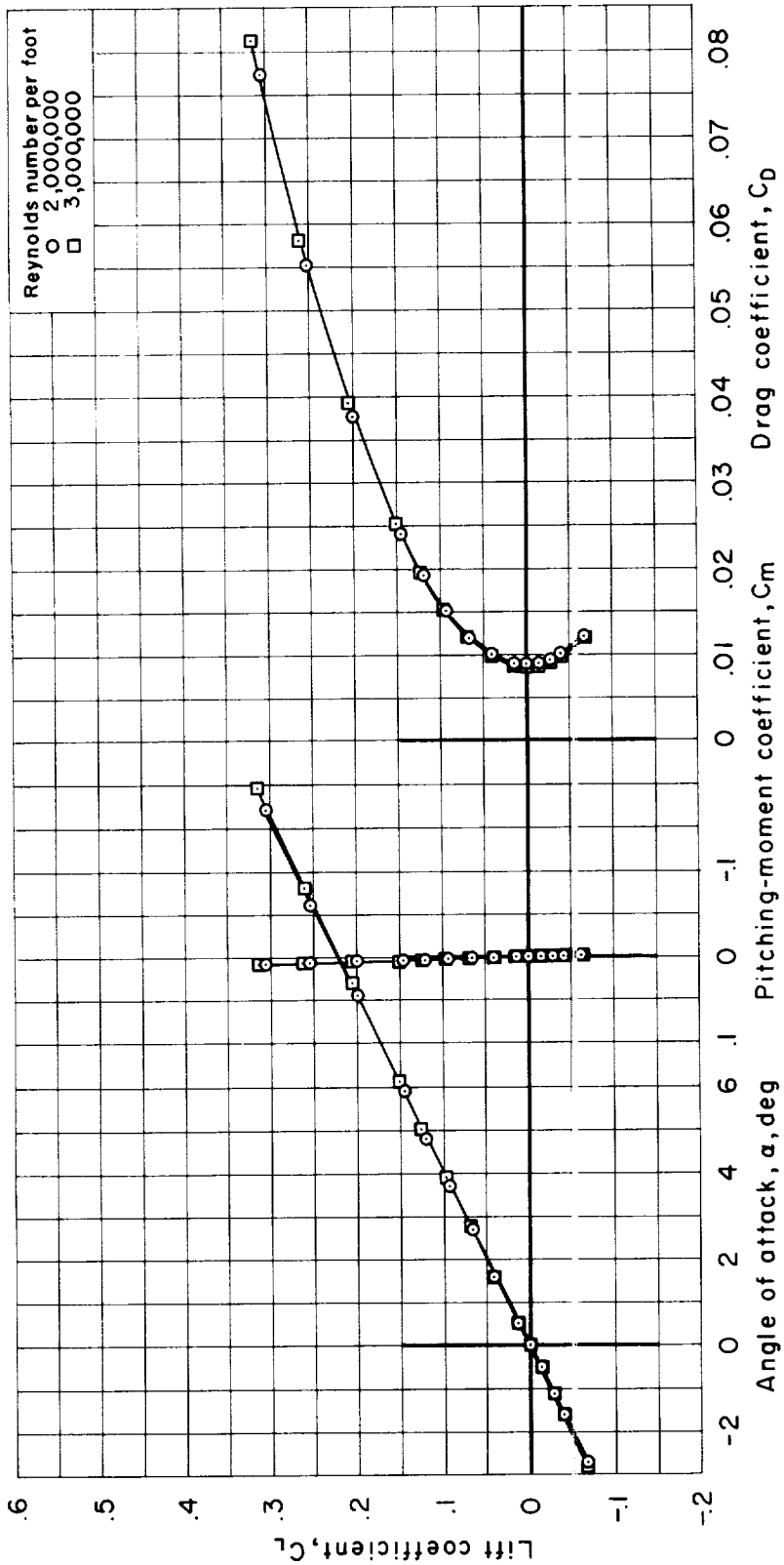

(d) Reynolds number effect at M = 3.00; curved delta model.

Figure 8.- Concluded.

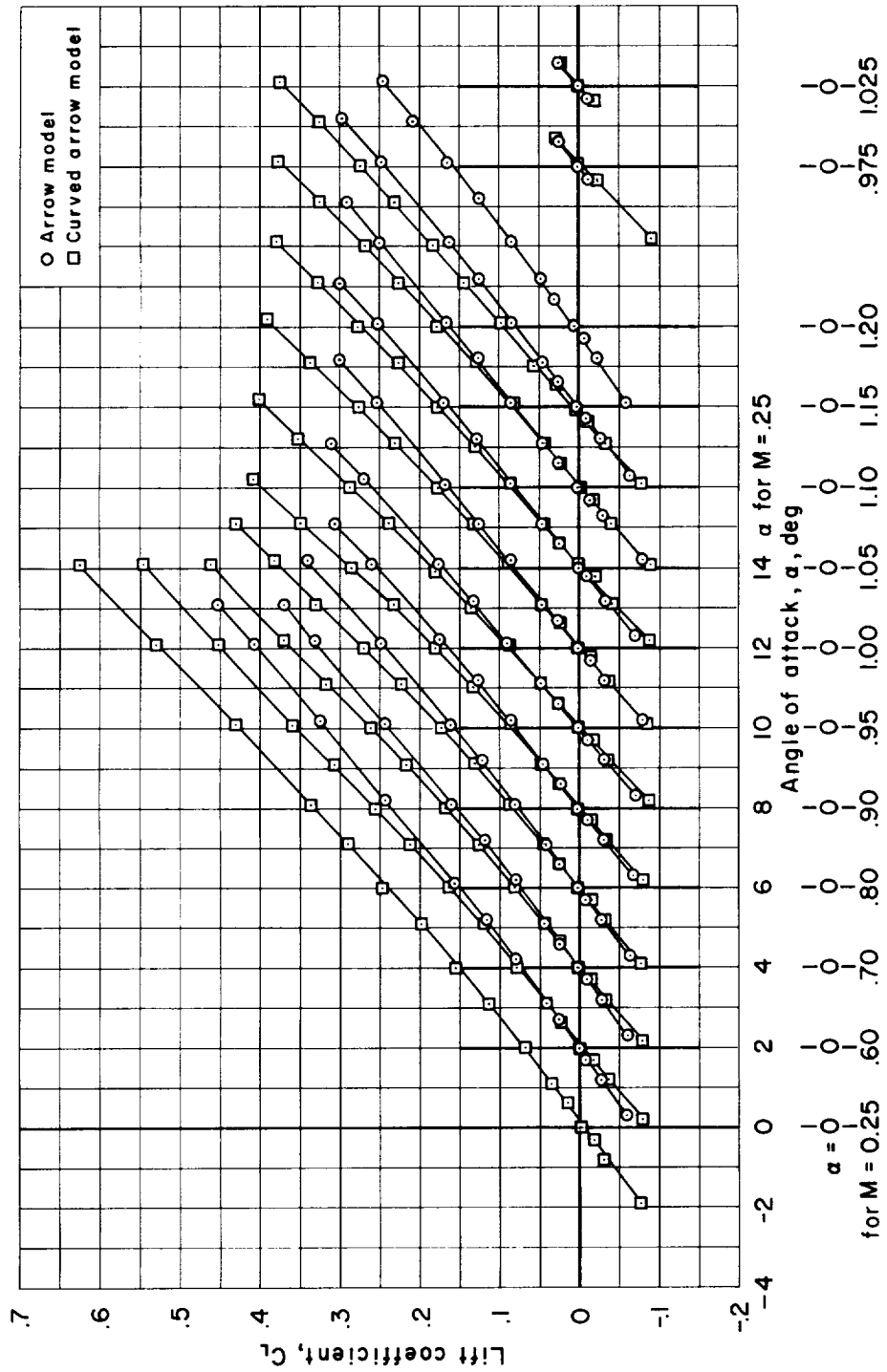

(a) C_L vs. α

Figure 9.- Transonic aerodynamic characteristics for the arrow and curved arrow models (R/ft = 1,800,000 to 4,000,000).

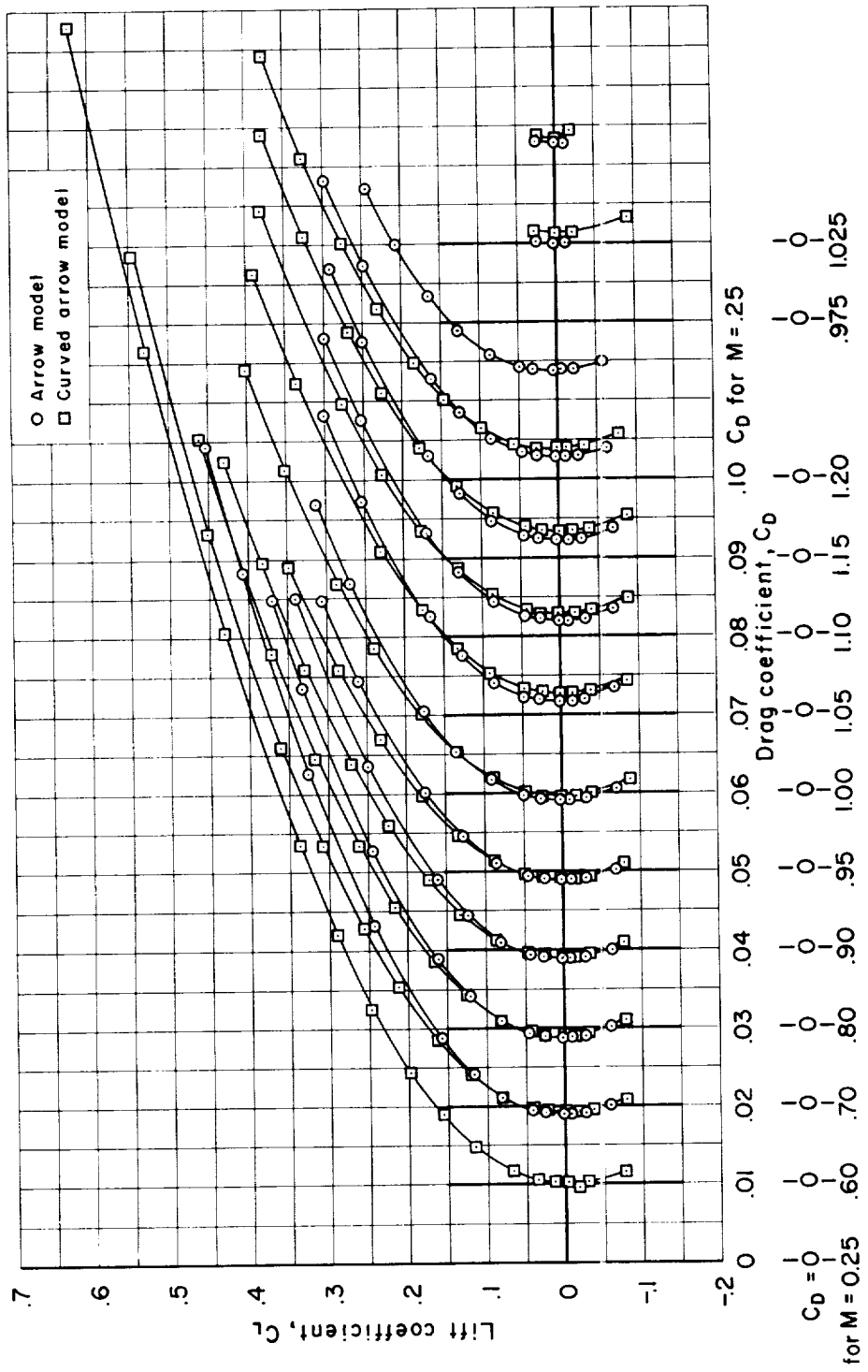

(b) C_L vs. C_D

Figure 9.- Continued.

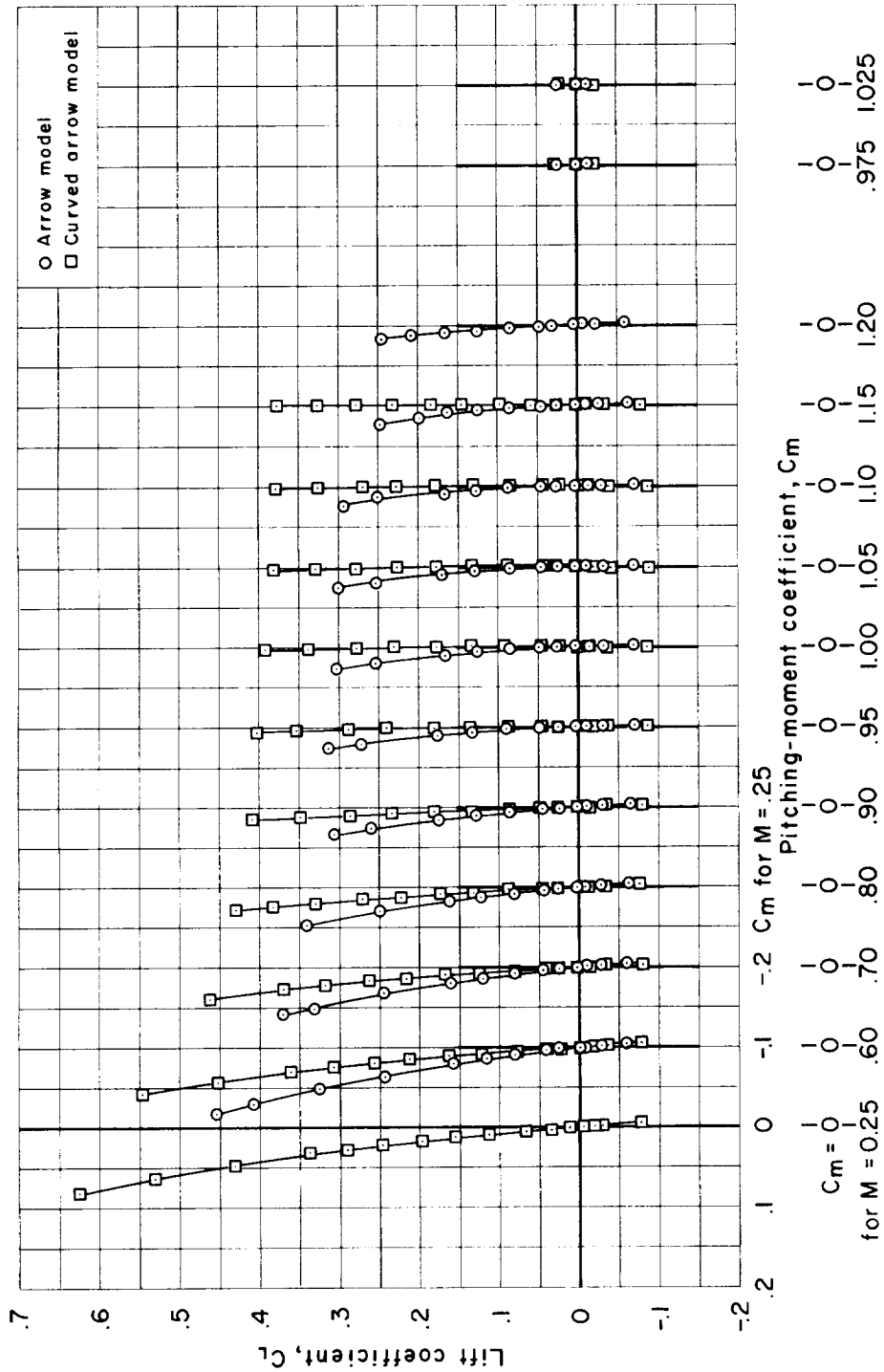

(c) C_L vs. C_m

Figure 9.- Continued.

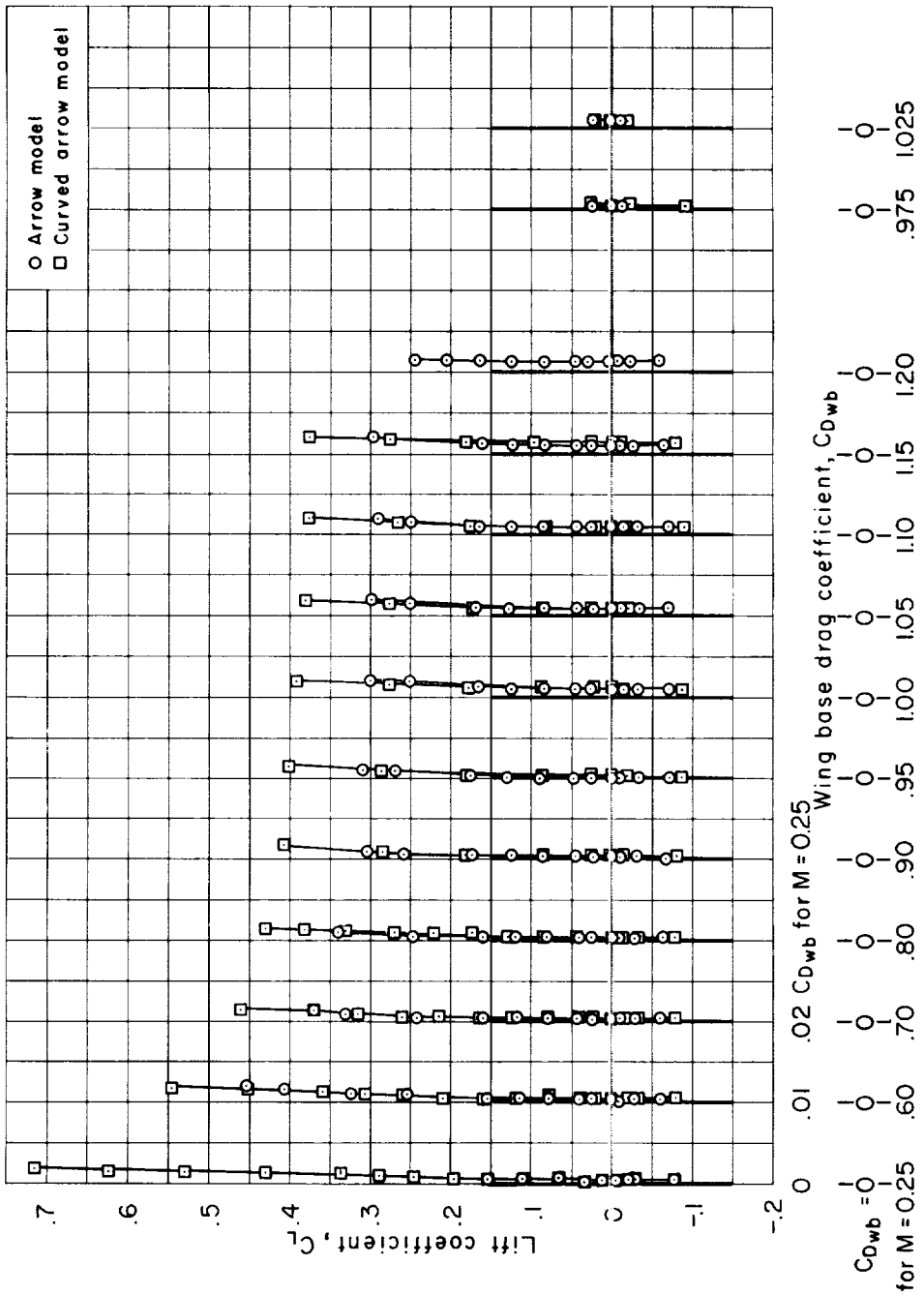

(d) C_L vs. $C_{D_{wb}}$

Figure 9.- Concluded.

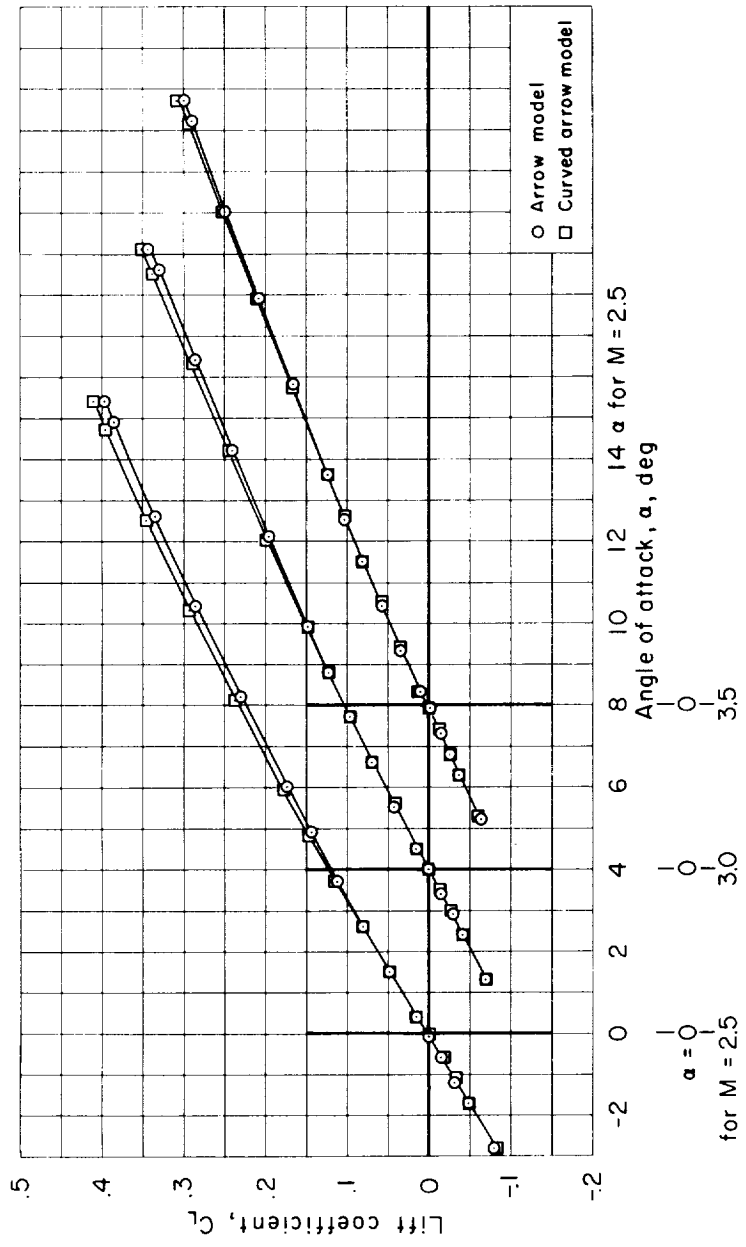

(a) C_L vs. α

Figure 10.- Supersonic aerodynamic characteristics for the arrow and curved arrow models (R/ft = 2,000,000).

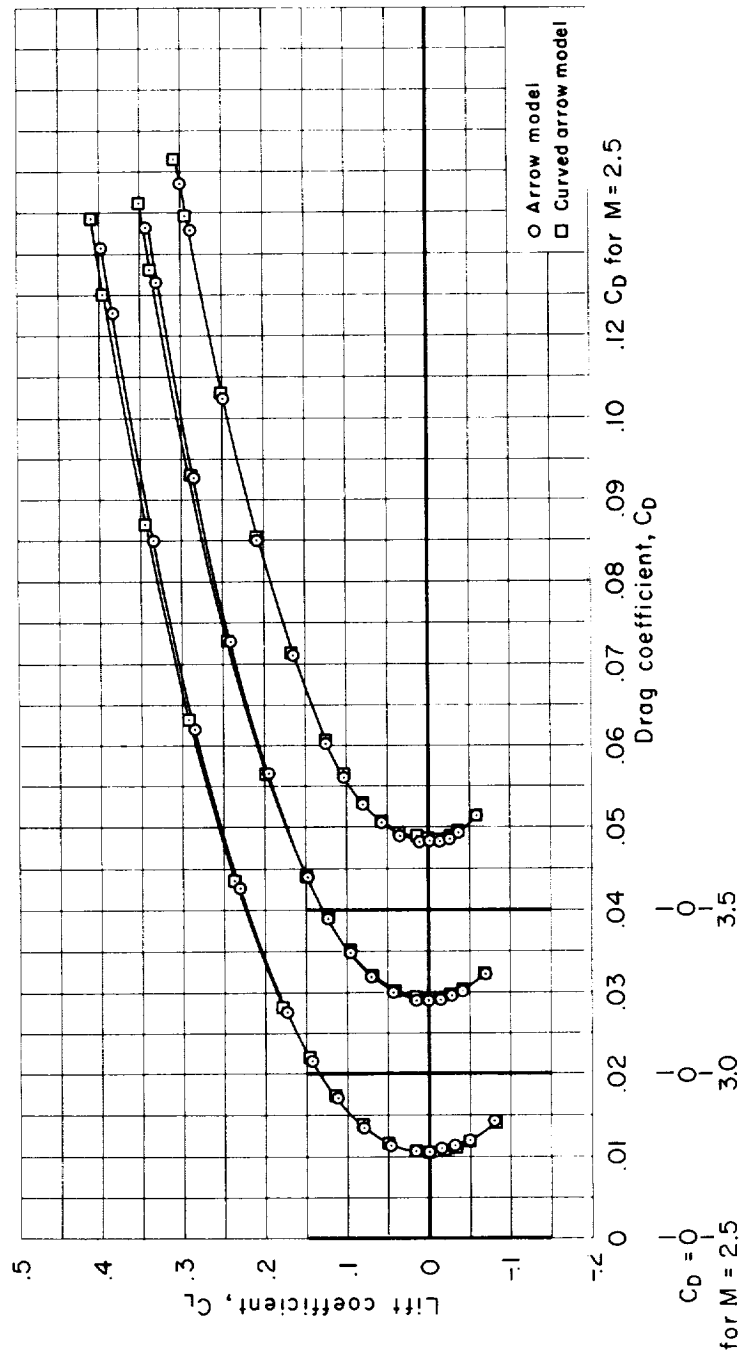

(b) C_L vs. C_D

Figure 10.- Continued.

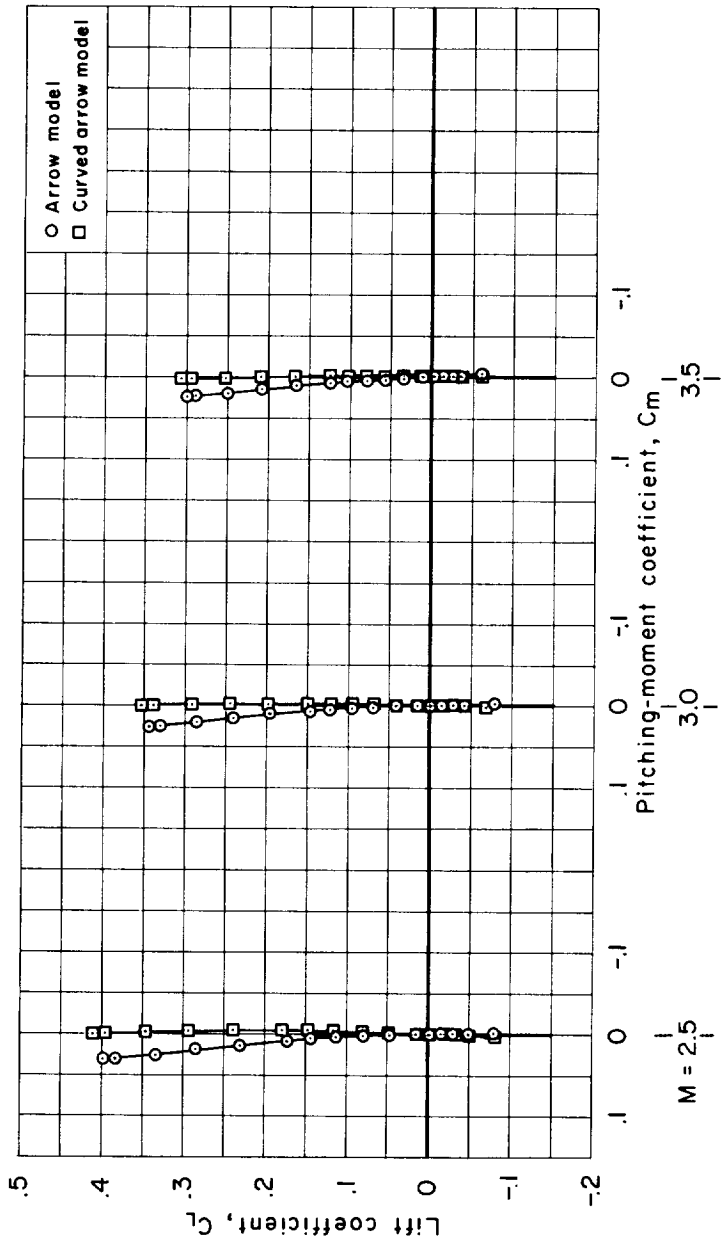

(c) C_L vs. C_m

Figure 10.- Continued.

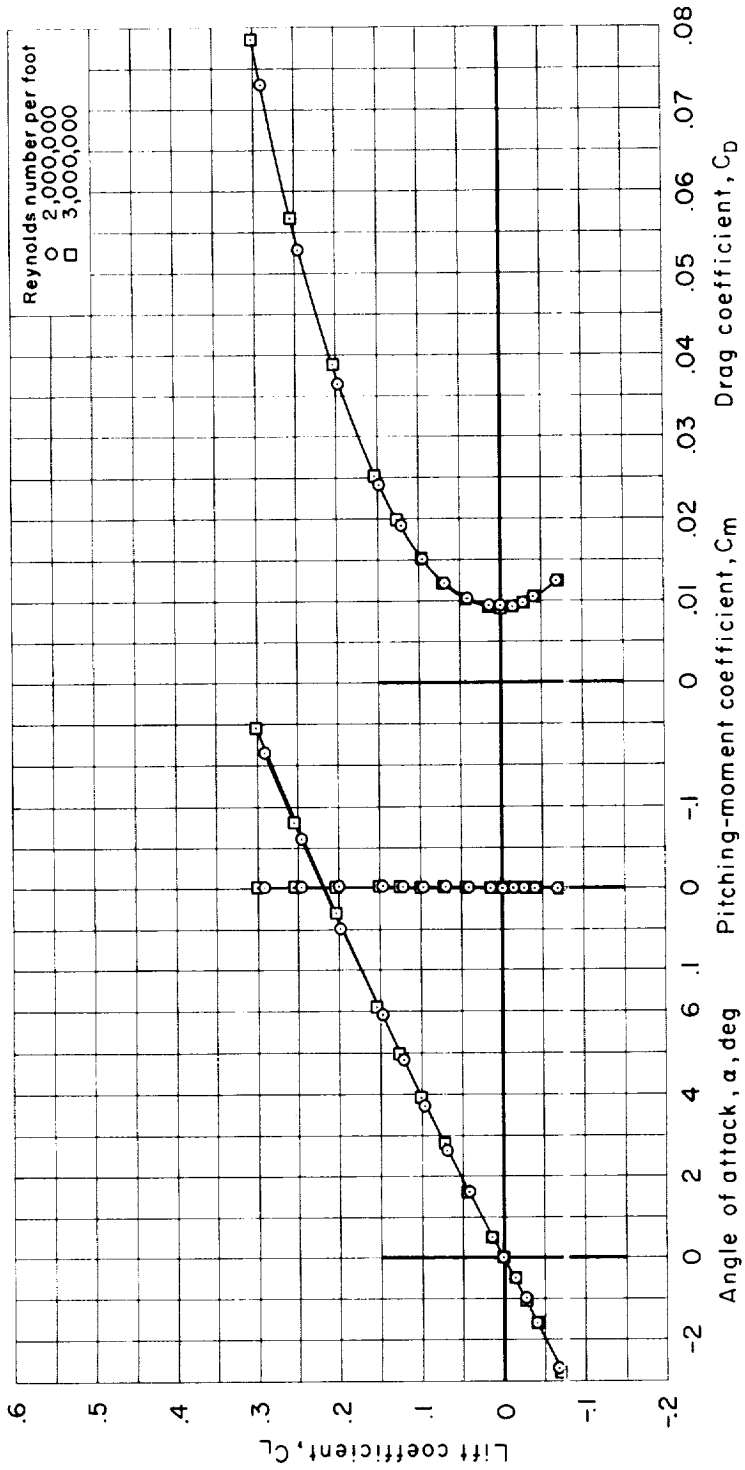

(d) Reynolds number effect at M = 3.00; curved arrow model.

Figure 10.- Concluded.

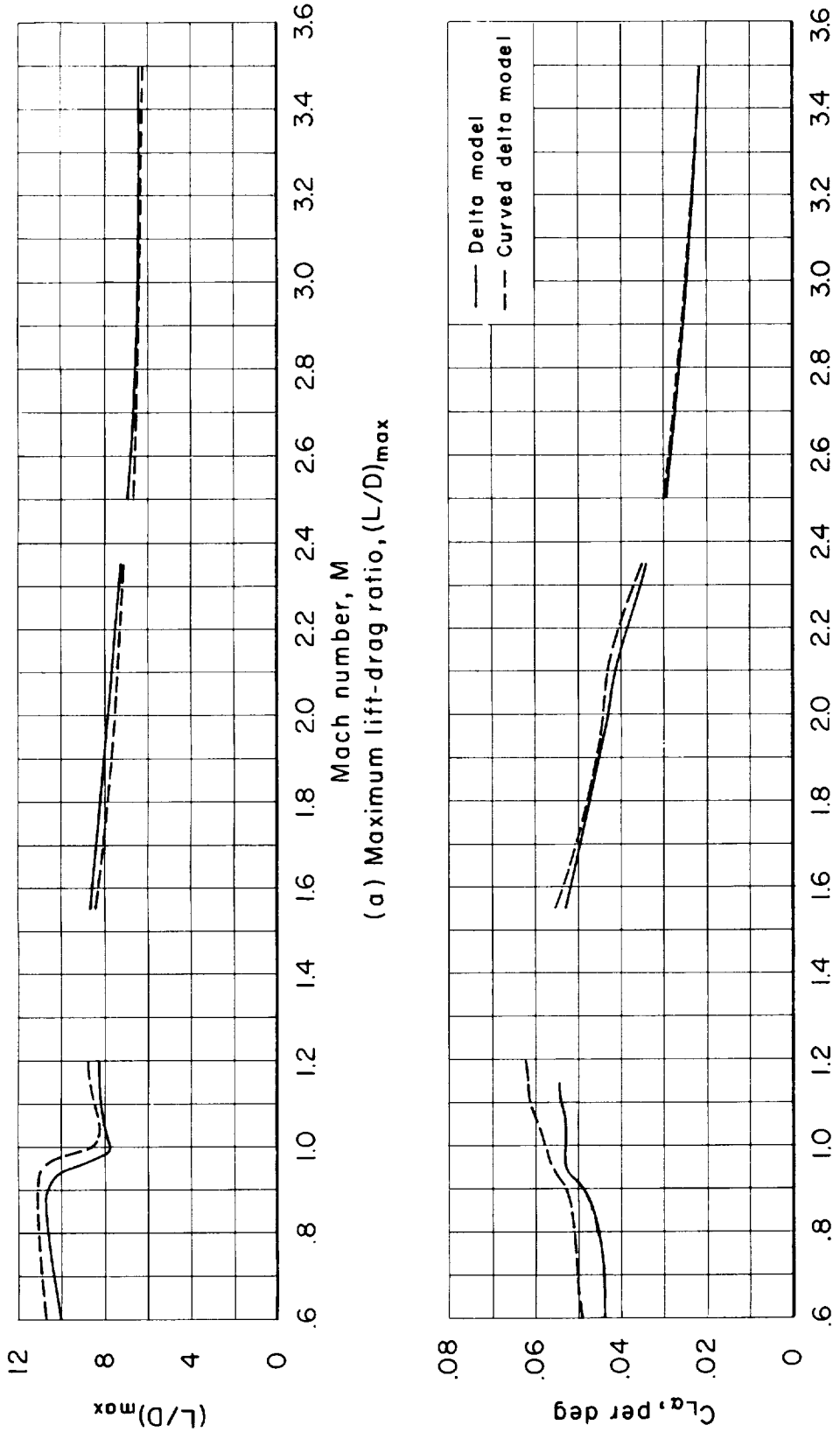

Figure 11.- Experimental aerodynamic trends with Mach number for the delta and curved delta models; transition fixed.

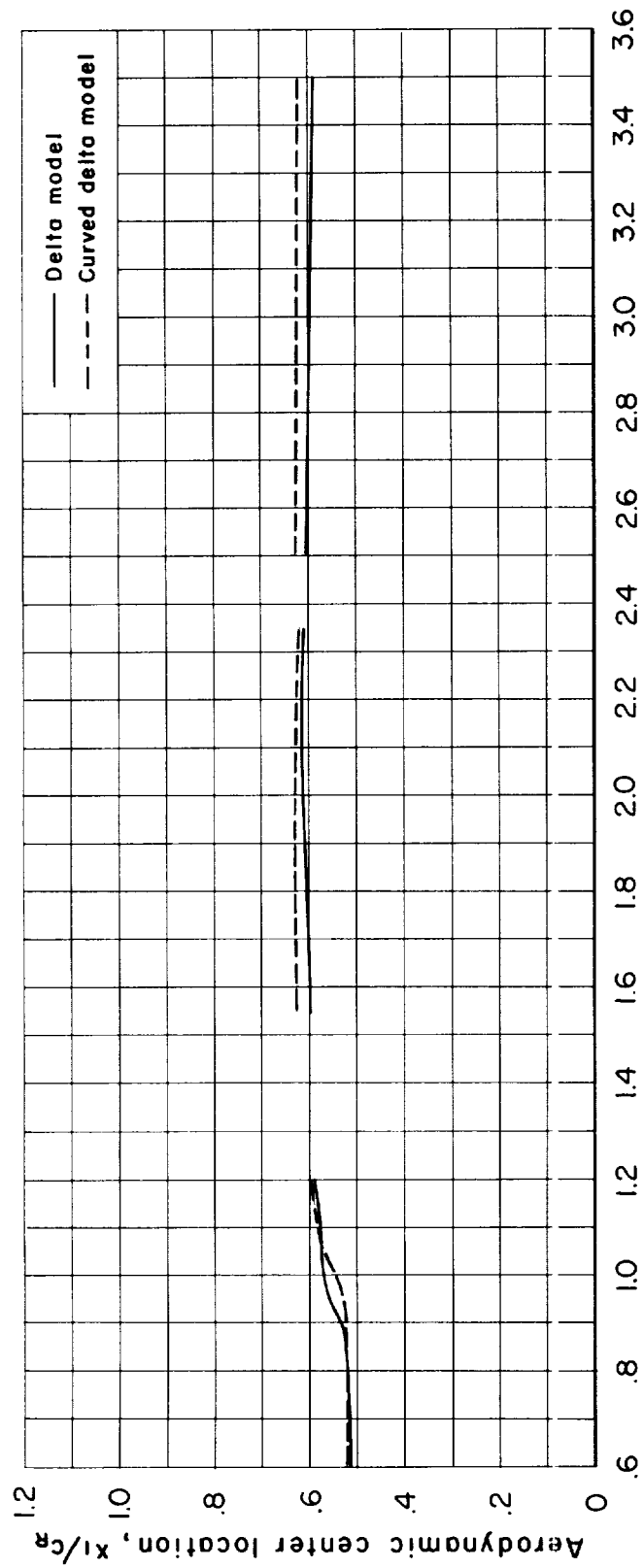

(c) Aerodynamic center location, x_1/c_R

Figure 11.- Concluded.

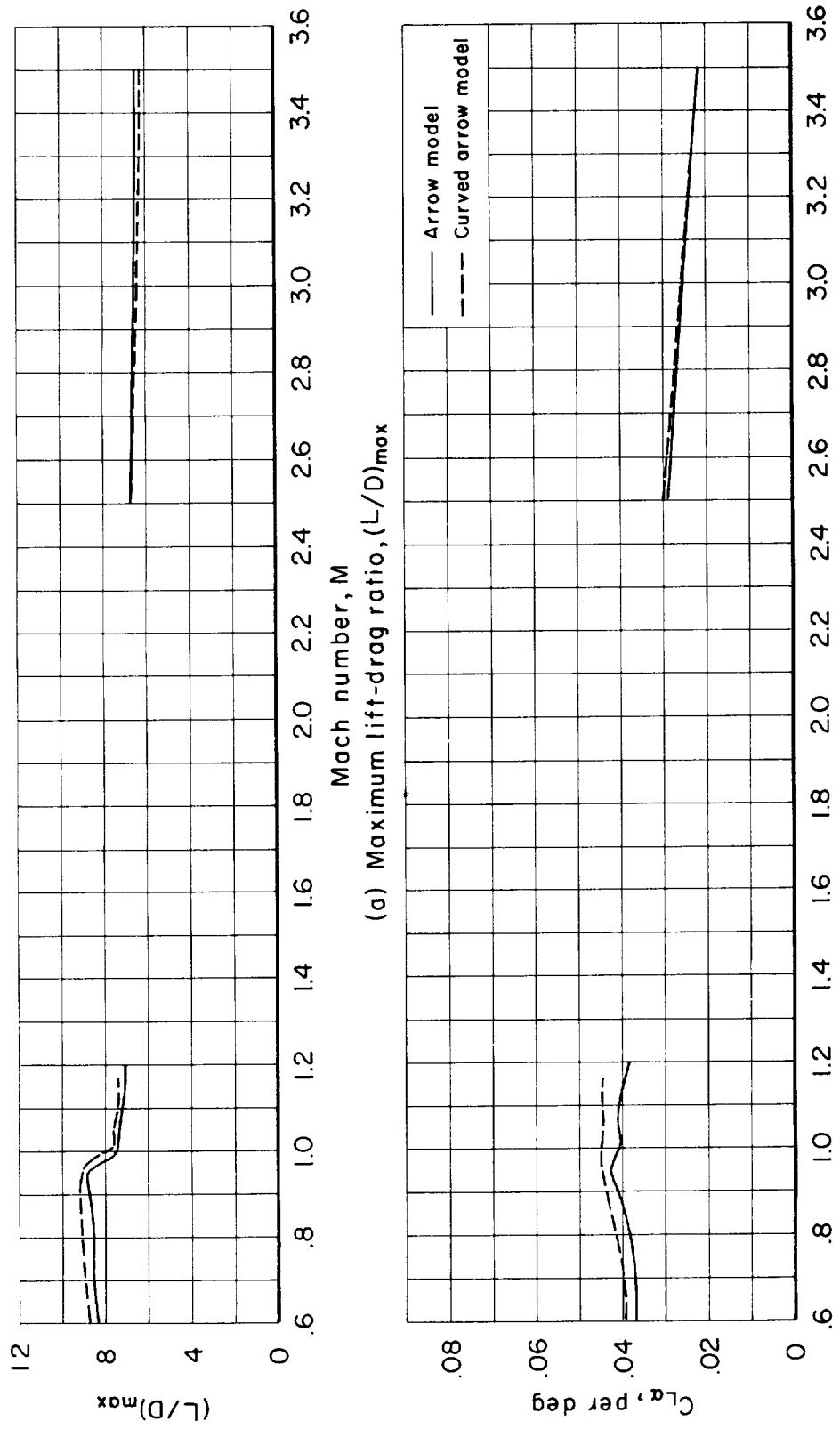

Figure 12.- Experimental aerodynamic trends with Mach number for the arrow and curved arrow models; transition fixed.

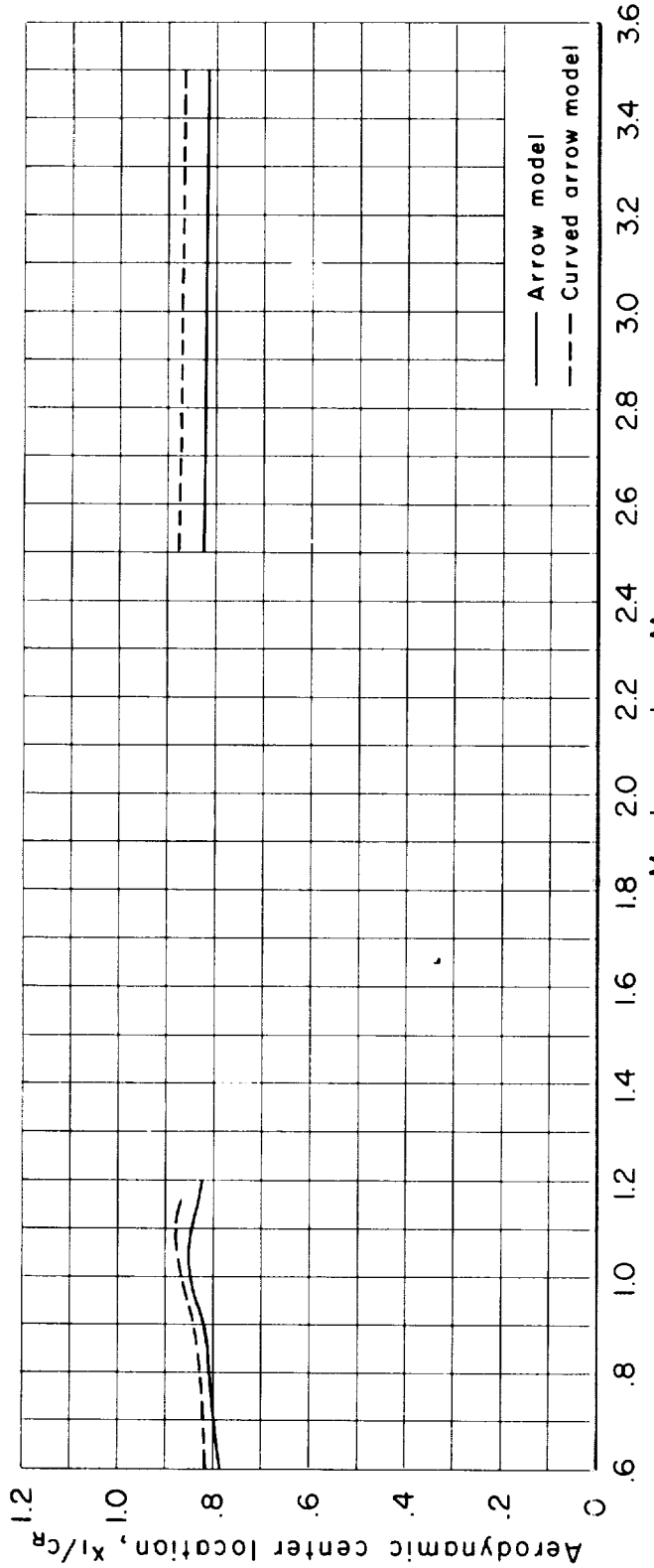

(c) Aerodynamic center location, x_1/c_R

Figure 12.- Concluded.

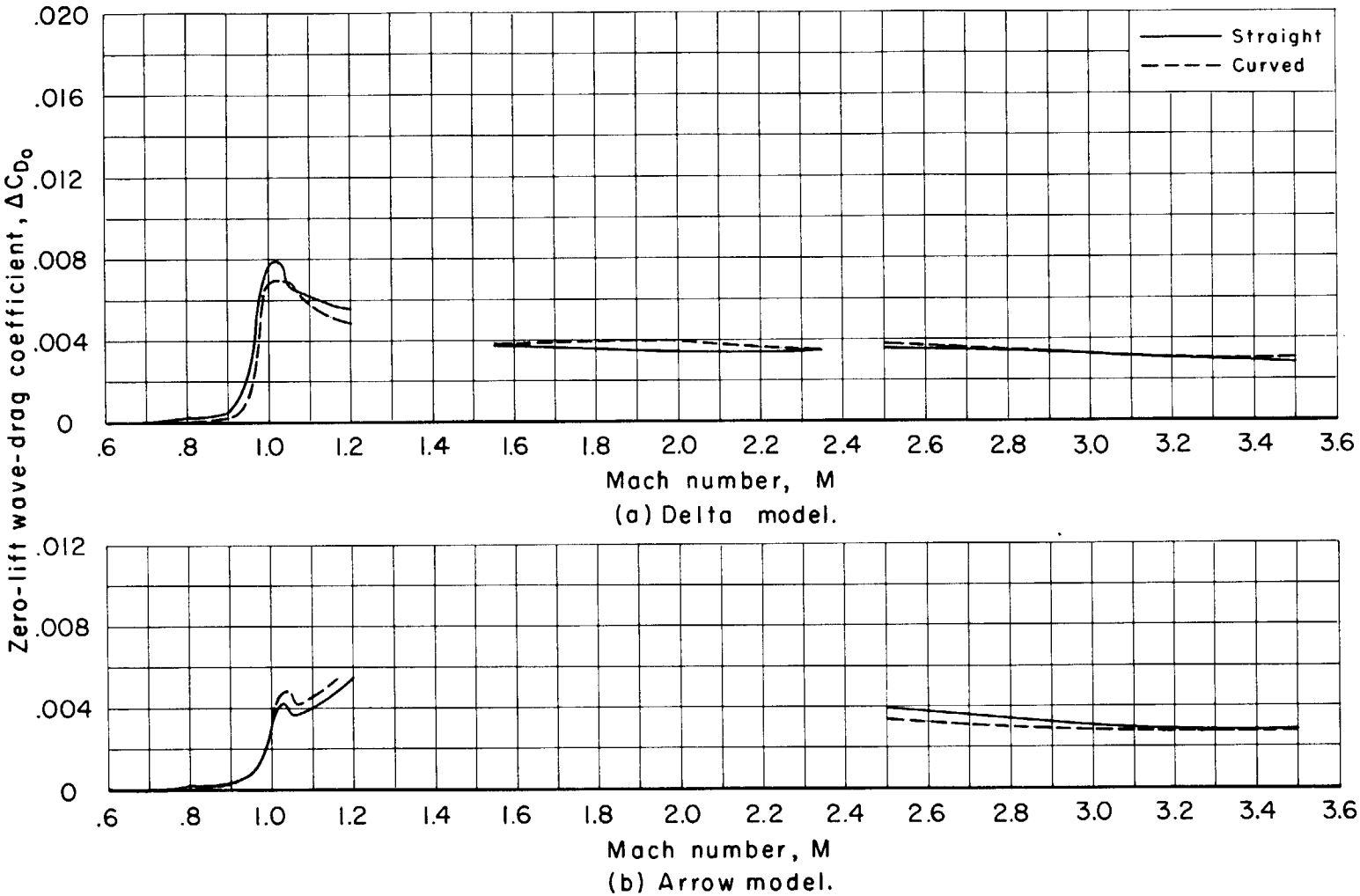

Figure 13.- Experimental zero-lift wave-drag coefficients of the straight and curved models.

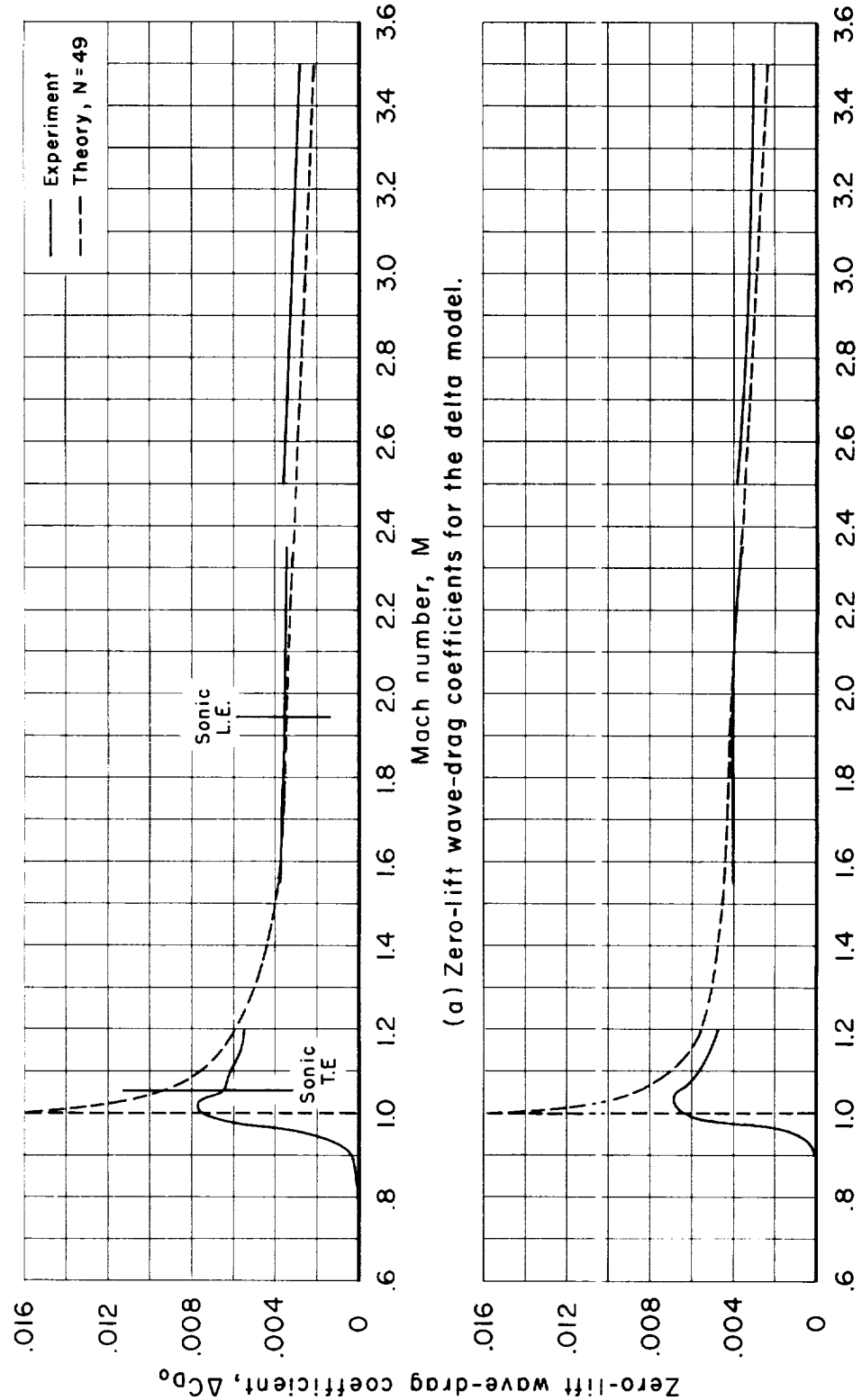

Figure 14.- Zero-lift wave-drag coefficients of the delta and curved delta models as determined by experiment and theory.

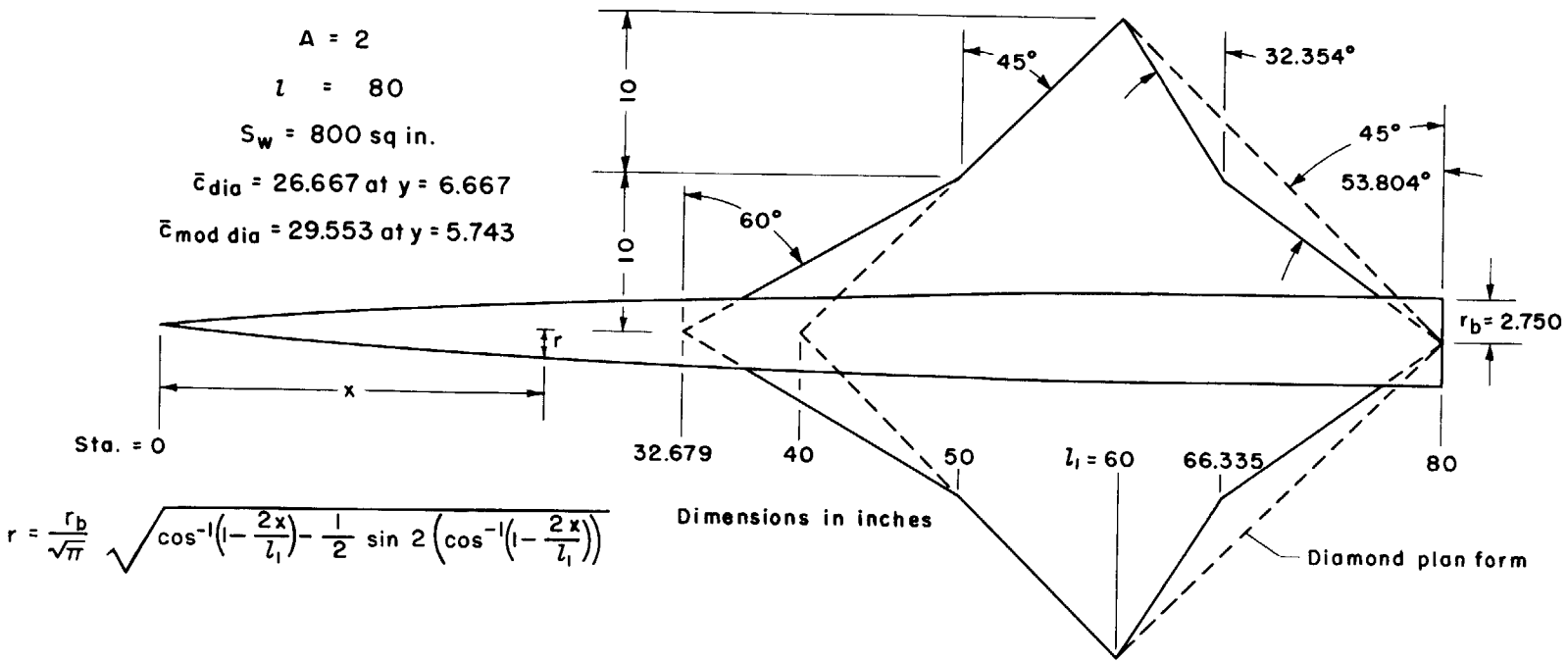

Figure 15.- Hypothetical models (diamond and modified diamond) selected to demonstrate potential wave-drag improvements.

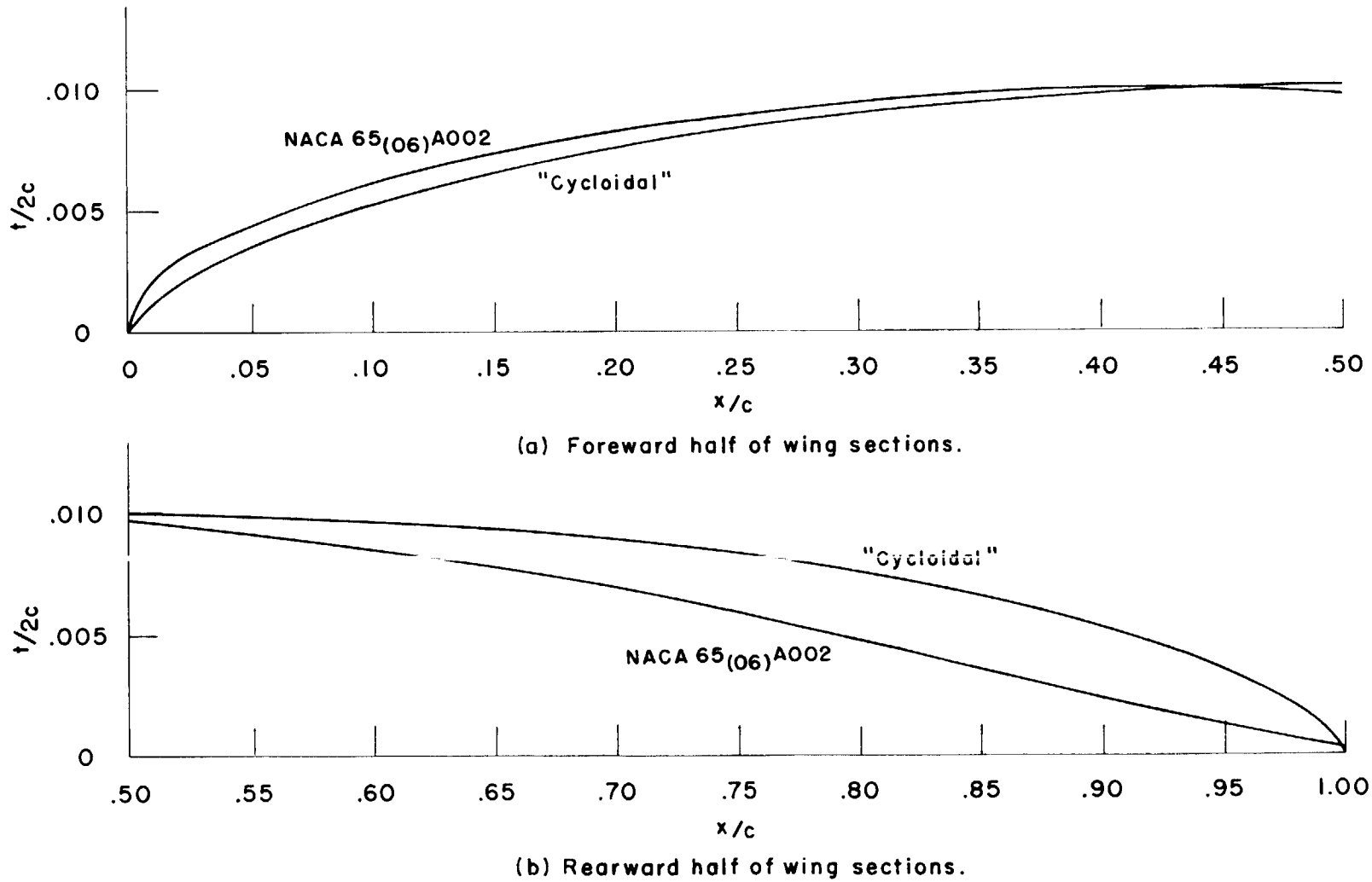

Figure 16.- The "cycloidal" and NACA 65(06)A002 wing sections.

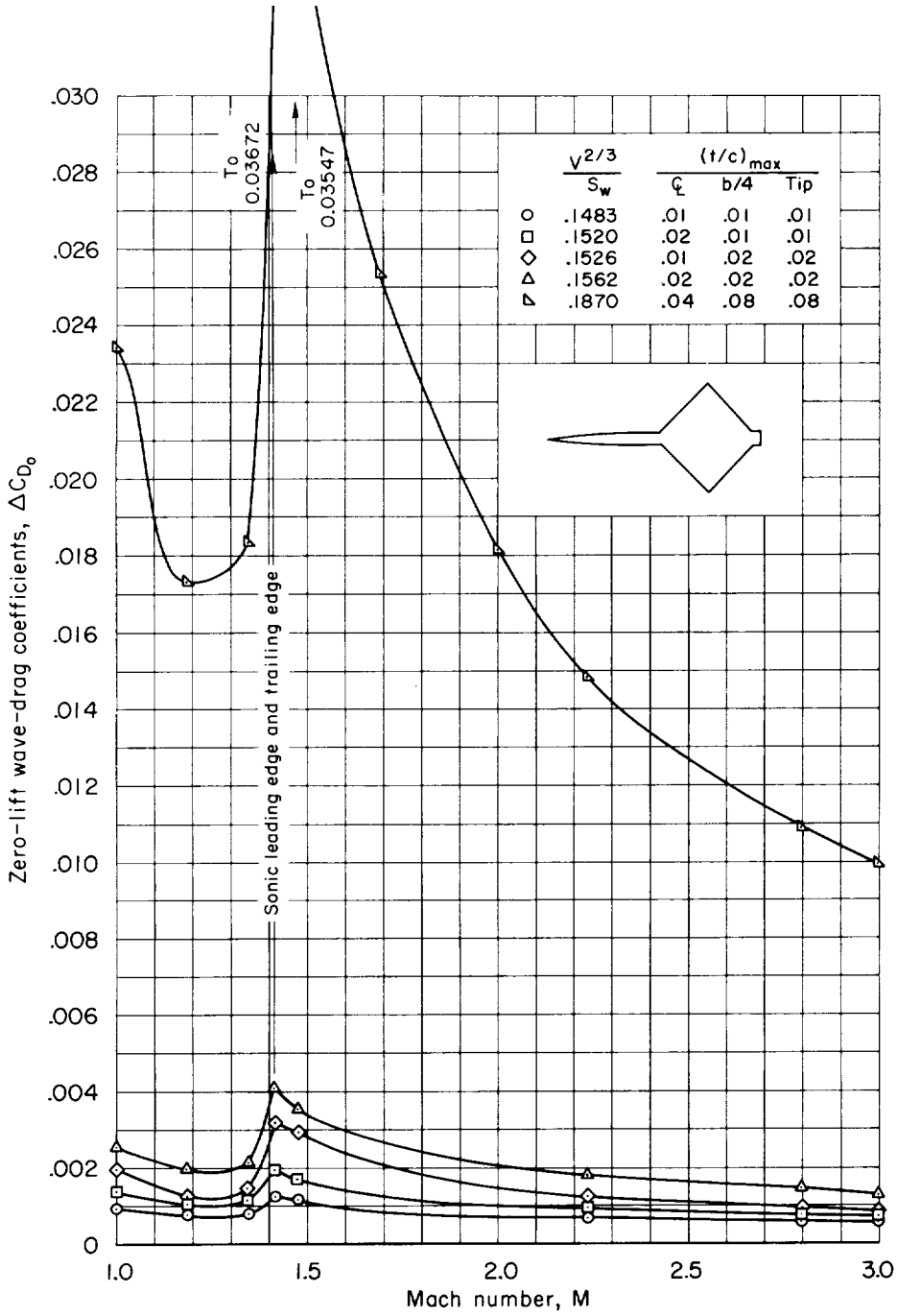

(a) Diamond model with "cycloidal" sections

Figure 17.- Theoretical zero-lift wave-drag coefficients for the hypothetical models with various wing section shapes and thickness (N=49).

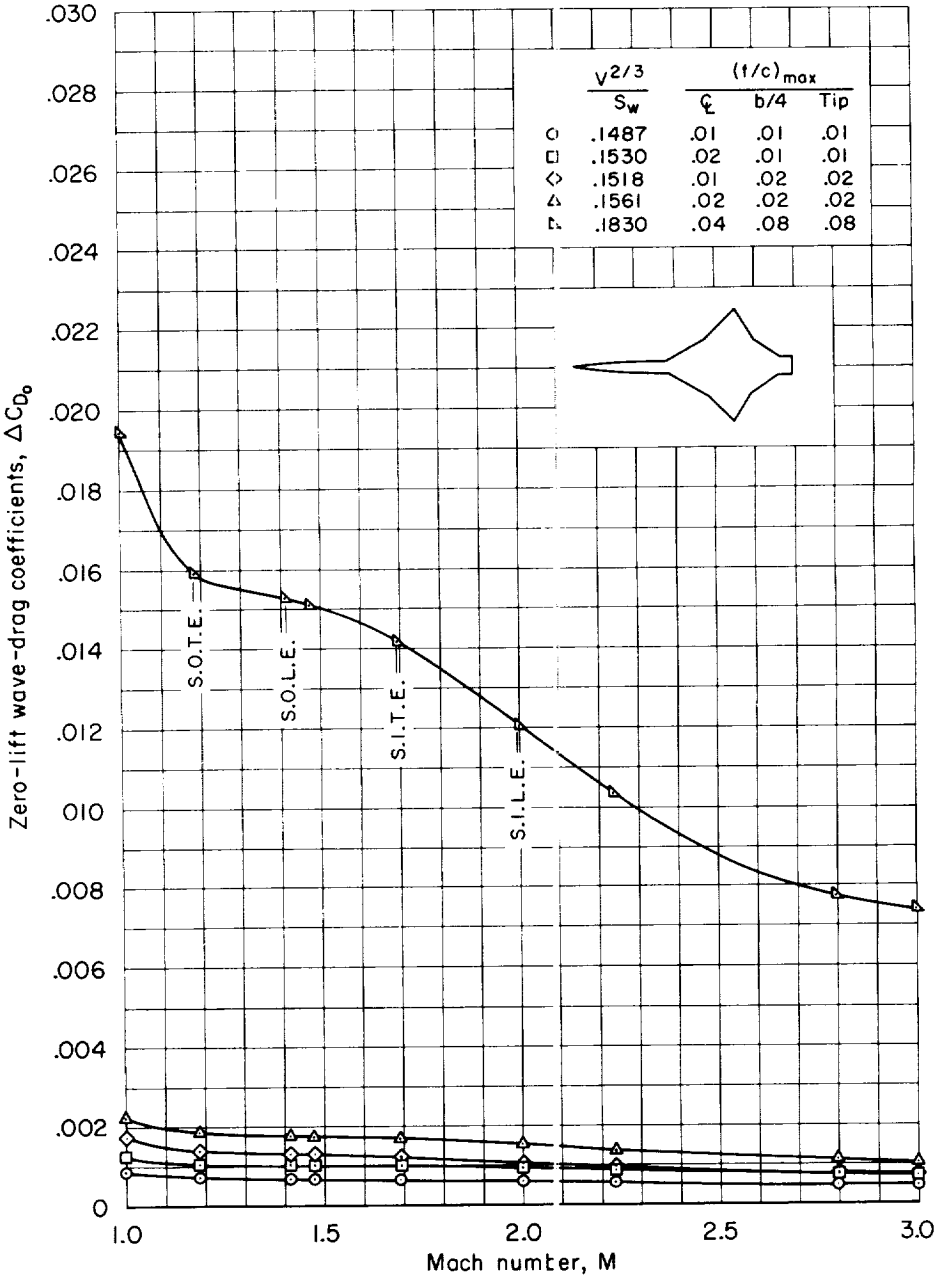

(b) Modified diamond model with "cycloidal" sections.

Figure 17.- Continued.

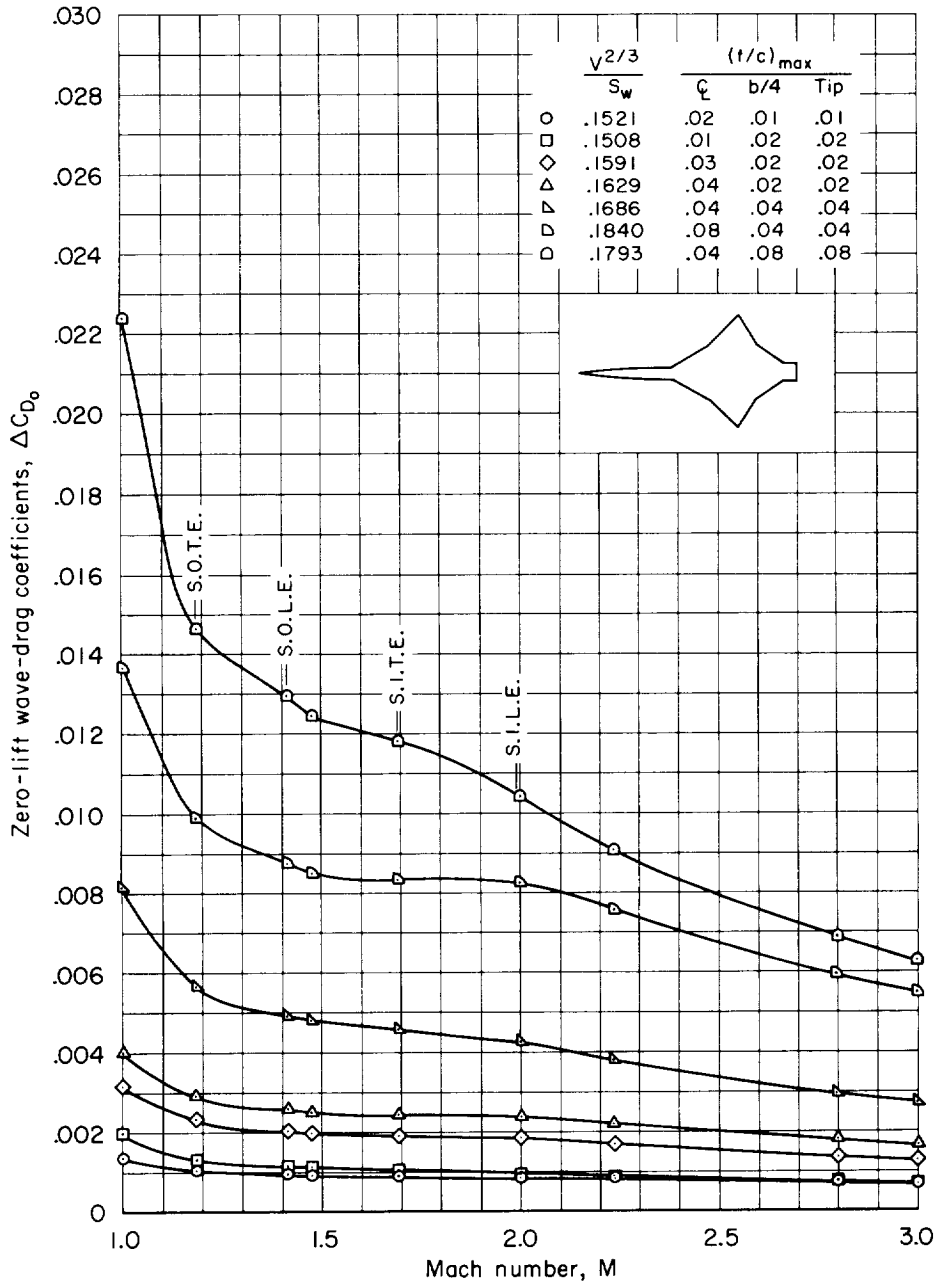

(c) Modified diamond model with 65(06)A00X sections.

Figure 17.- Concluded.

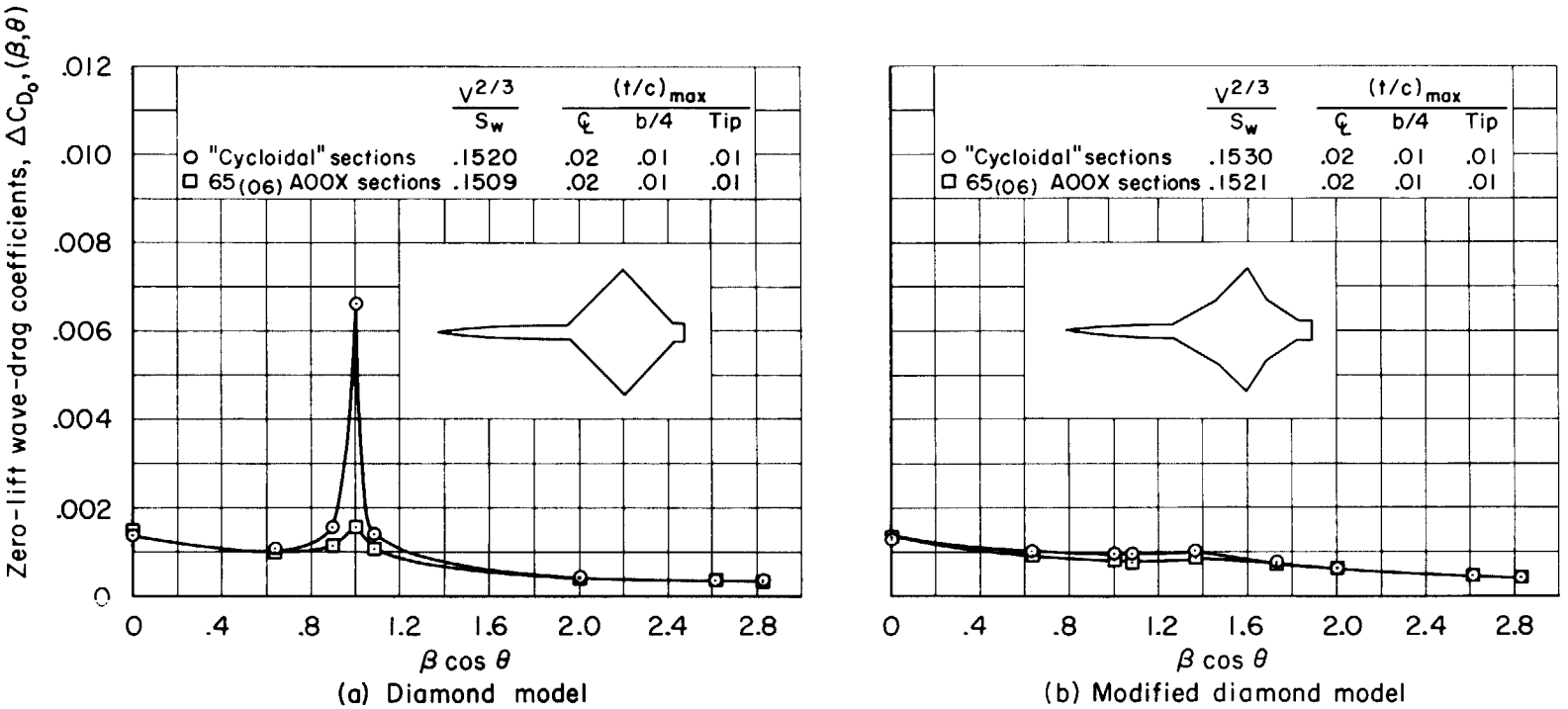

Figure 18.- Theoretical zero-lift wave-drag parameters determined as a function of $\beta \cos \theta$ for the hypothetical models with thin wing sections (N=49).

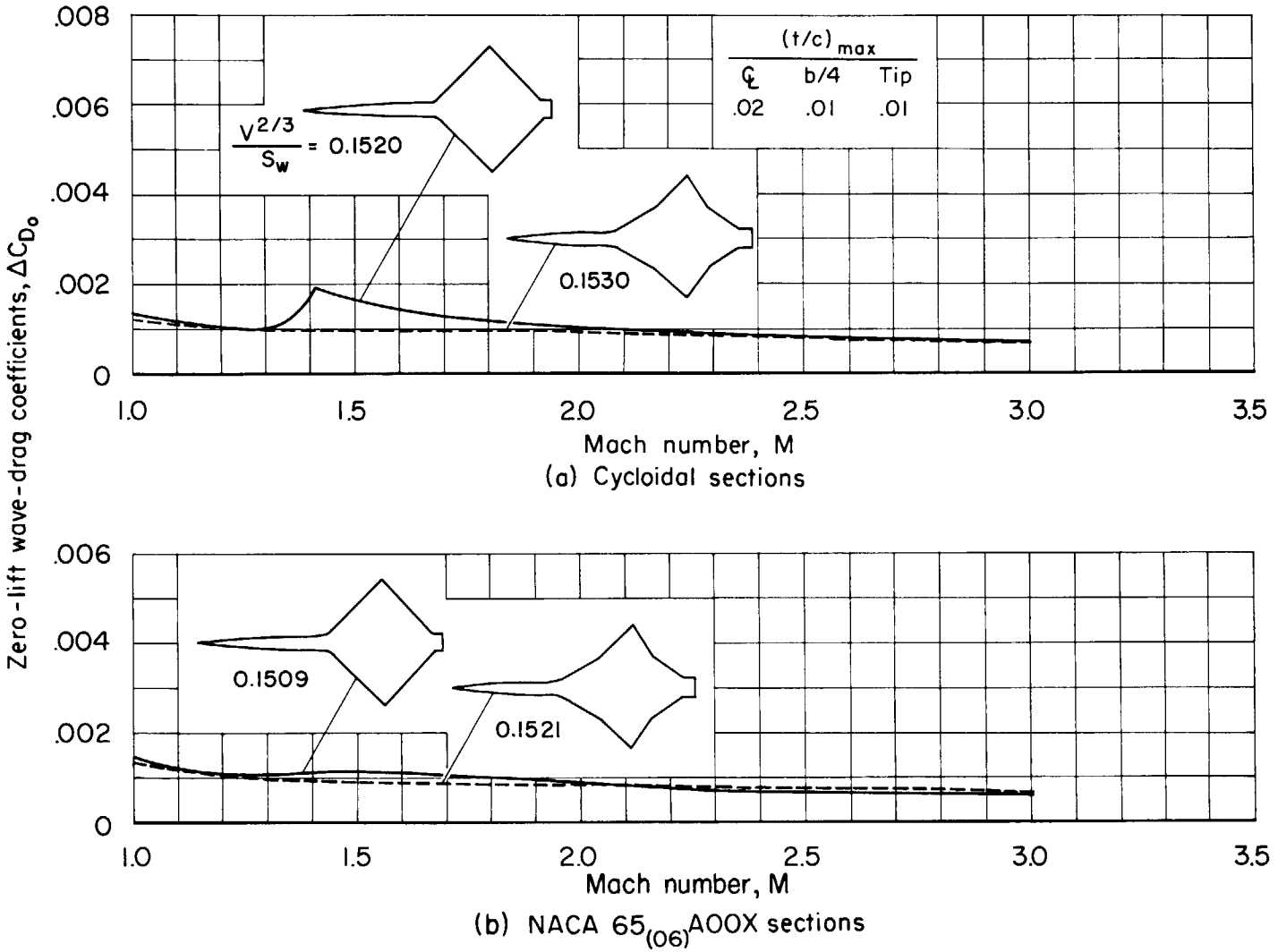

Figure 19.- Theoretical zero-lift wave-drag coefficients for the hypothetical models with thin wing sections (N=49).

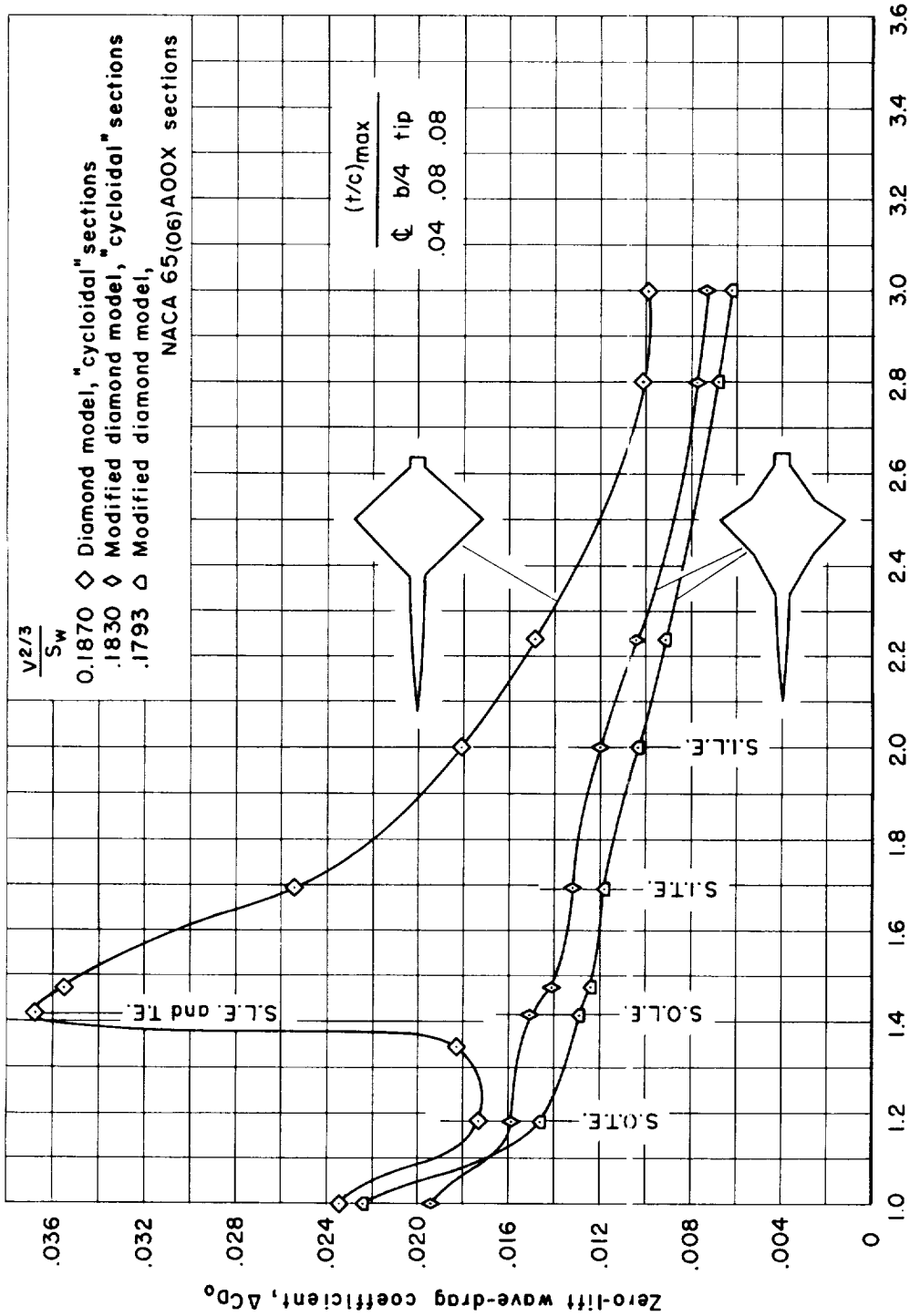

Figure 20.- Theoretical zero-lift wave-drag coefficients for the hypothetical models with thick wing sections (N=49).

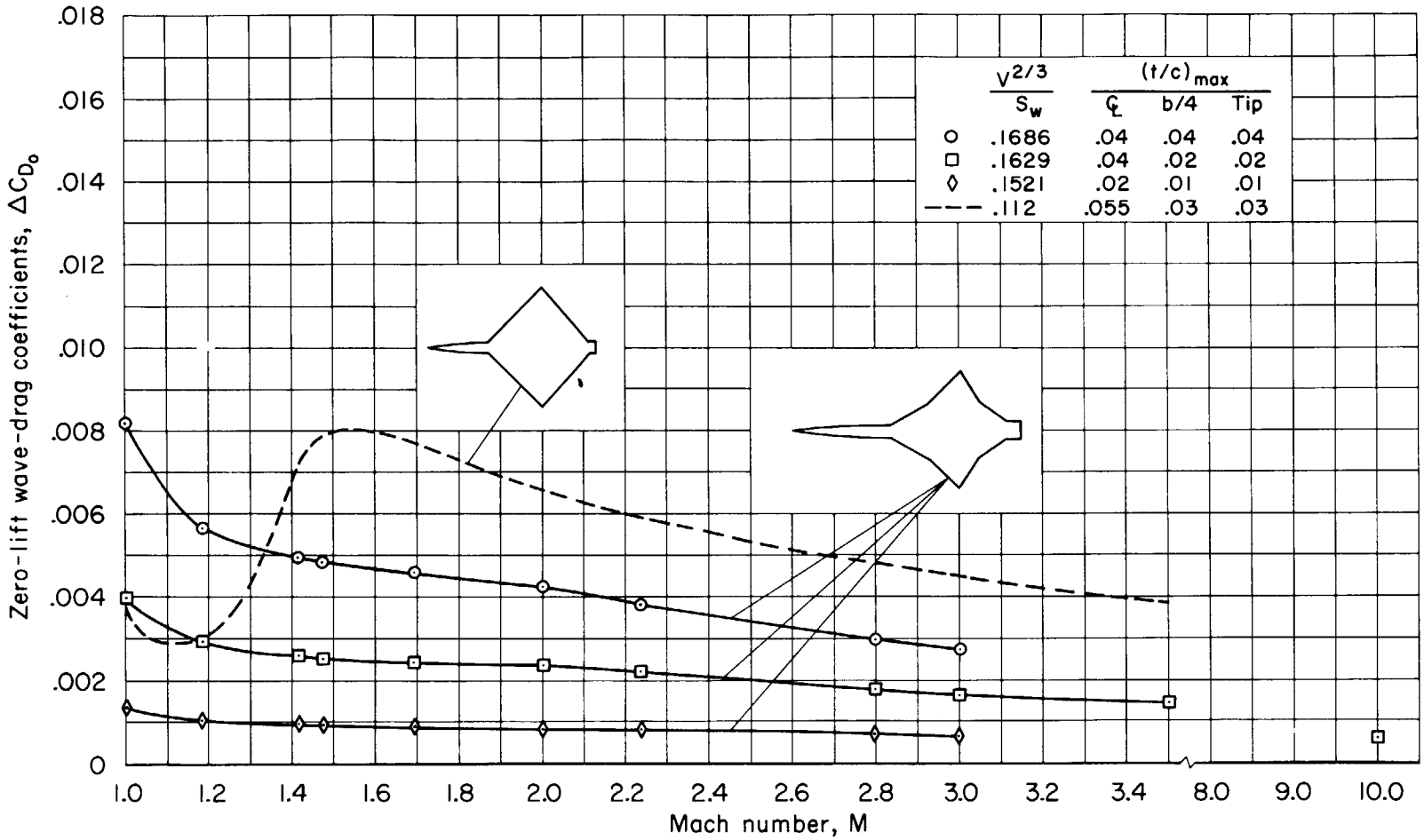

Figure 21.- Theoretical zero-lift wave-drag coefficients for the hypothetical modified-diamond model with several wing thicknesses and for the blended diamond wing-body combination (N=49).

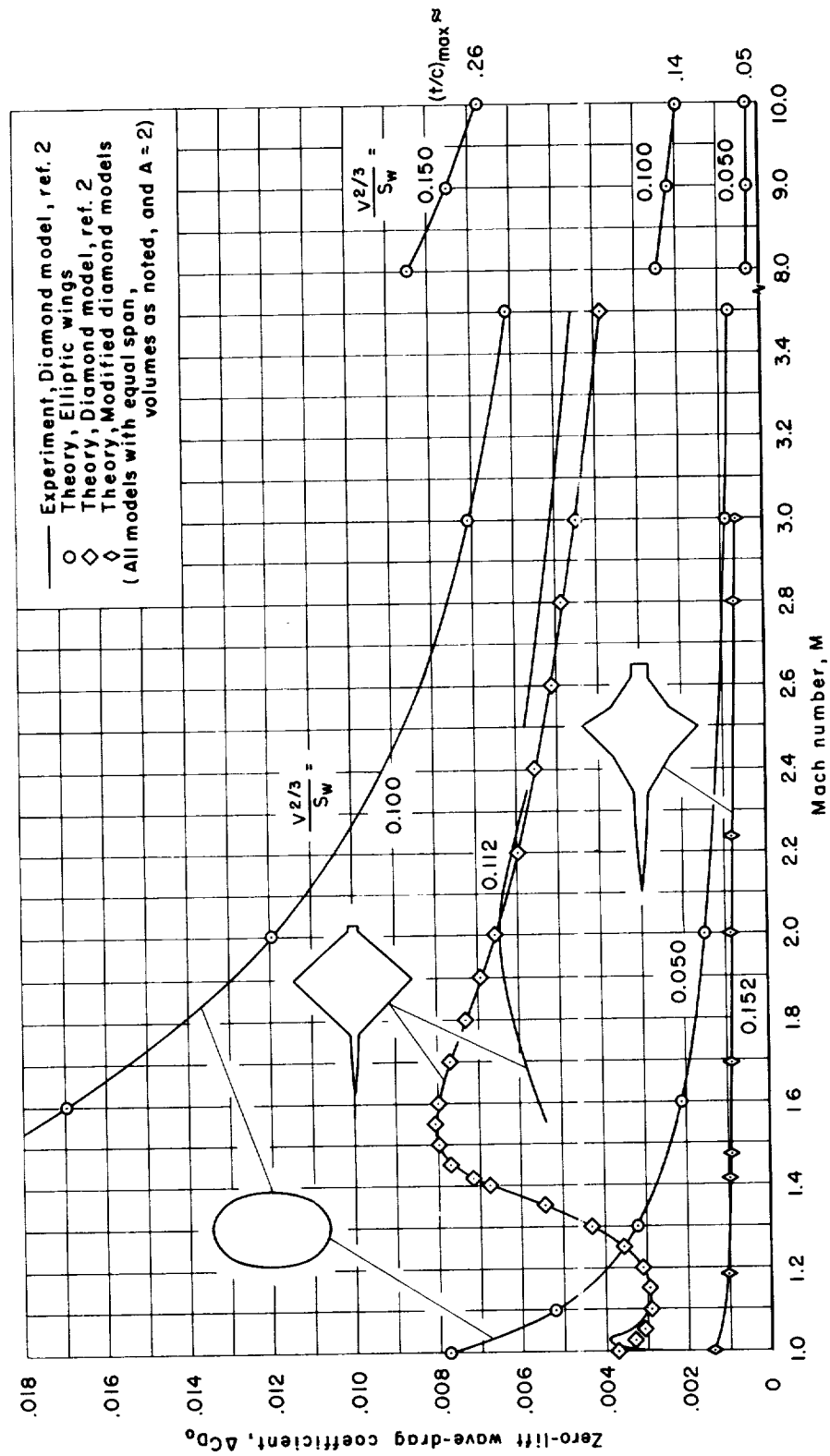

Figure 22.- Theoretical zero-lift wave-drag coefficients (N=49) for the hypothetical modified-diamond model, blended diamond model, and elliptic wings of comparable volume compared with experimental results from reference 2.

NASA TM X-379
National Aeronautics and Space Administration.
EVALUATION OF BLENDED WING-BODY COMBINATIONS WITH CURVED PLAN FORMS AT MACH NUMBERS UP TO 3.50. George H. Holdaway and Jack A. Mellenthin. October 1960. 66p.
(NASA TECHNICAL MEMORANDUM X-379)

(Title, Unclassified)

Aerodynamic data are presented for aspect-ratio-2 delta and arrow plan forms with curved leading and trailing edges. The leading-edge sweeps of comparable and previously tested straight-edged wings were 59.04^{o} and 70.82^{o}, respectively. The corresponding trailing-edge sweeps were -18.43^{o} and 41.19^{o}. The curved leading and trailing edges had the same average sweep as the straight edges. A modification to a diamond plan form which appears advantageous is discussed in an appendix.

Copies obtainable from NASA, Washington

I. Holdaway, George H.
II. Mellenthin, Jack A.
III. NASA TM X-379

(Initial NASA distribution: 3, Aircraft.)

NASA

NASA TM X-379
National Aeronautics and Space Administration.
EVALUATION OF BLENDED WING-BODY COMBINATIONS WITH CURVED PLAN FORMS AT MACH NUMBERS UP TO 3.50. George H. Holdaway and Jack A. Mellenthin. October 1960. 66p.
(NASA TECHNICAL MEMORANDUM X-379)

(Title, Unclassified)

Aerodynamic data are presented for aspect-ratio-2 delta and arrow plan forms with curved leading and trailing edges. The leading-edge sweeps of comparable and previously tested straight-edged wings were 59.04^{o} and 70.82^{o}, respectively. The corresponding trailing-edge sweeps were -18.43^{o} and 41.19^{o}. The curved leading and trailing edges had the same average sweep as the straight edges. A modification to a diamond plan form which appears advantageous is discussed in an appendix.

Copies obtainable from NASA, Washington

I. Holdaway, George H.
II. Mellenthin, Jack A.
III. NASA TM X-379

(Initial NASA distribution: 3, Aircraft.)

NASA

NASA TM X-379
National Aeronautics and Space Administration.
EVALUATION OF BLENDED WING-BODY COMBINATIONS WITH CURVED PLAN FORMS AT MACH NUMBERS UP TO 3.50. George H. Holdaway and Jack A. Mellenthin. October 1960. 66p.
(NASA TECHNICAL MEMORANDUM X-379)

(Title, Unclassified)

Aerodynamic data are presented for aspect-ratio-2 delta and arrow plan forms with curved leading and trailing edges. The leading-edge sweeps of comparable and previously tested straight-edged wings were 59.04^{o} and 70.82^{o}, respectively. The corresponding trailing-edge sweeps were -18.43^{o} and 41.19^{o}. The curved leading and trailing edges had the same average sweep as the straight edges. A modification to a diamond plan form which appears advantageous is discussed in an appendix.

Copies obtainable from NASA, Washington

I. Holdaway, George H.
II. Mellenthin, Jack A.
III. NASA TM X-379

(Initial NASA distribution: 3, Aircraft.)

NASA

NASA TM X-379
National Aeronautics and Space Administration.
EVALUATION OF BLENDED WING-BODY COMBINATIONS WITH CURVED PLAN FORMS AT MACH NUMBERS UP TO 3.50. George H. Holdaway and Jack A. Mellenthin. October 1960. 66p.
(NASA TECHNICAL MEMORANDUM X-379)

(Title, Unclassified)

Aerodynamic data are presented for aspect-ratio-2 delta and arrow plan forms with curved leading and trailing edges. The leading-edge sweeps of comparable and previously tested straight-edged wings were 59.04^{o} and 70.82^{o}, respectively. The corresponding trailing-edge sweeps were -18.43^{o} and 41.19^{o}. The curved leading and trailing edges had the same average sweep as the straight edges. A modification to a diamond plan form which appears advantageous is discussed in an appendix.

Copies obtainable from NASA, Washington

I. Holdaway, George H.
II. Mellenthin, Jack A.
III. NASA TM X-379

(Initial NASA distribution: 3, Aircraft.)

NASA